

1 **Impact of HO₂ aerosol uptake on radical levels and O₃** 2 **production during summertime in Beijing**

Style Definition: Heading 2

Style Definition: Heading 3

3 Joanna E. Dyson¹, Lisa K. Whalley^{1,2*}, Eloise J. Slater^{1,a}, Robert Woodward-Massey¹,
4 Chunxiang Ye³, James D. Lee^{4,5}, Freya Squires^{4,b}, James R. Hopkins^{4,5}, Rachel E. Dunmore⁴,
5 Marvin Shaw^{4,5}, Jacqueline F. Hamilton⁴, Alastair C. Lewis^{4,5}, Stephen D. Worrall⁶, Asan
6 Bacak⁷, Archit Mehra^{8,c}, Thomas J. Bannan⁸, Hugh Coe^{8,9}, Carl J. Percival¹⁰, Bin Ouyang¹¹, C.
7 Nicholas Hewitt¹¹, Roderic L. Jones¹², Leigh R. Crilley¹³, Louisa J. Kramer¹⁴, W. Joe. F.
8 Acton¹⁴, William J. Bloss¹⁴, Supattarachai Saksakulkrai¹⁴, Jingsha Xu^{14,d}, Zongbo Shi¹⁴, Roy
9 M. Harrison^{14,e}, Simone Kotthaus^{15,16}, Sue Grimmond¹⁵, Yele Sun¹⁷, Weiqi Xu¹⁷, Siyao
10 Yue^{17,18,19}, Lianfang Wei^{17,19}, Pingqing Fu^{17,18}, Xinming Wang²⁰, Stephen R. Arnold²¹,
11 Dwayne E. Heard^{1*}

12 *[1] School of Chemistry, University of Leeds, LS2 9JT, UK.*

13 *[2] National Centre of Atmospheric Science, University of Leeds, LS2 9JT, UK.*

14 *[3] College of Environmental Sciences and Engineering, Peking University, Beijing, 100871,*
15 *China.*

16 *[4] Wolfson Atmospheric Chemistry Laboratories, Department of Chemistry, University of*
17 *York, Heslington, York, YO10 5DD, UK.*

18 *[5] National Centre of Atmospheric Science, University of York, Heslington, York, YO19 5DD,*
19 *UK.*

20 *[6] Aston Institute of Materials Research, School of Engineering and Applied Science, Aston*
21 *University, Birmingham, B4 7ET, UK.*

22 *[7] Turkish Accelerator and Radiation Laboratory, Ankara University Institute of Accelerator*
23 *Technologies, Atmospheric and Environmental Chemistry Laboratory, Gölbaşı Campus,*
24 *Ankara, Turkey.*

25 *[8] Centre of Atmospheric Sciences, School of Earth and Environmental Sciences, University*
26 *of Manchester, Manchester, M13 9PL, UK.*

27 *[9] National Centre for Atmospheric Sciences, University of Manchester, Manchester, M13*
28 *9PL, UK.*

- 29 [10] *Jet Propulsion Laboratory, California Institute of Technology, Pasadena, CA, USA.*
- 30 [11] *Lancaster Environment Centre, Lancaster University, Lancaster, LA1 4YW, UK.*
- 31 [12] *Department of Chemistry, University of Cambridge, Cambridge, UK.*
- 32 [13] *Department of Chemistry, York University, Toronto, ON, M3J 1P3, Canada.*
- 33 [14] *School of Geography, Earth and Environmental Sciences, University of Birmingham,*
34 *Birmingham, B15 2TT, UK.*
- 35 [15] *Department of Meteorology, University of Reading, Reading, UK.*
- 36 [16] *Institut Pierre Simon Laplace, École Polytechnique, Palaiseau, France.*
- 37 [17] *State Key Laboratory of Atmospheric Boundary Layer Physics and Atmospheric*
38 *Chemistry, Institute for Atmospheric Physics, Chinese Academy of Sciences, Beijing 100029,*
39 *China.*
- 40 [18] *Institute of Surface-Earth System Science, School of Earth System Science, Tianjin*
41 *University, Tianjin 300072, China.*
- 42 [19] *Minerva Research Group, Max Planck Institute for Chemistry, 55128 Mainz, Germany.*
- 43 [20] *State Key Laboratory of Organic Geochemistry, Guangzhou Institute of Geochemistry,*
44 *Chinese Academy of Sciences, Guangzhou, 510640, China.*
- 45 [21] *School of Earth and Environment, University of Leeds, LS2 9JT, UK.*
- 46 ^a*now at: The Hut Group, Unit 1 Icon Manchester, Manchester Airport, WA15 0AF, UK.*
- 47 ^b*now at: British Antarctic Survey, Cambridge, CB3 0ET, UK.*
- 48 ^c*now at: Chaucer, Part of Bip Group, 10 Lower Thames Street, London, EC3R 6EN^d*
49 *now at: Beijing Hanzhou Innovation Institute Yuhang, Xixi Octagon City, Yuhang District, Hangzhou*
50 *310023, China.*
- 51 ^e*also at: Department of Environmental Sciences, Faculty of Meteorology, Environment and*
52 *Arid Land Agriculture, King Abdulaziz University, Jeddah, Saudi Arabia.*
- 53 **Correspondence to: D.E.Heard@leeds.ac.uk, L.K.Whalley@leeds.ac.uk*

54

55

56 **Abstract** The impact of heterogeneous uptake of HO₂ onto aerosol surfaces on radical
57 concentrations and the O₃ production regime in Beijing summertime was investigated. The
58 uptake coefficient of HO₂ onto aerosol surfaces, γ_{HO_2} , was calculated for the AIRPRO
59 campaign in Beijing, Summer 2017, as a function of measured aerosol soluble copper
60 concentration, [Cu²⁺]_{eff}, aerosol liquid water content, [ALWC], and particulate matter
61 concentration, [PM]. An average γ_{HO_2} across the entire campaign of 0.070 ± 0.035 was
62 calculated, with values ranging from 0.002 to 0.15, and found to be significantly lower than
63 the value of $\gamma_{HO_2} = 0.2$, commonly used in modelling studies. Using the calculated γ_{HO_2} values
64 for the Summer AIRPRO campaign, OH, HO₂ and RO₂ radical concentrations were modelled
65 using a box-model incorporating the Master Chemical Mechanism (v3.3.1), with and without
66 the addition of γ_{HO_2} , and compared to the measured radical concentrations. Rate of destruction
67 analysis showed the dominant HO₂ loss pathway to be HO₂ + NO for all NO concentrations
68 across the Summer Beijing campaign with HO₂ uptake contributing < 0.3 % to the total loss of
69 HO₂ on average. This result for Beijing summertime would suggest that under most conditions
70 encountered, HO₂ uptake onto aerosol surfaces is not important to consider when investigating
71 increasing O₃ production with decreasing [PM] across the North China Plain. At low [NO],
72 however, i.e. < 0.1 ppb, which was often encountered in the afternoons, up to 29% of modelled
73 HO₂ loss was due to HO₂ uptake on aerosols when calculated γ_{HO_2} was included, even with the
74 much lower γ_{HO_2} values compared to $\gamma_{HO_2} = 0.2$, a results which agrees with the aerosol-
75 inhibited O₃ regime recently proposed by Ivatt et al., 2022. As such it can be concluded that in
76 cleaner environments, away from polluted urban centres where HO₂ loss chemistry is not
77 dominated by NO but where aerosol surface area is high still, changes in PM concentration and
78 hence aerosol surface area could still have a significant effect on both overall HO₂
79 concentration and the O₃ production regime.

80 Using modelled radical concentrations, the absolute O₃ sensitivity to NO_x and VOC showed
81 that, on average across the summer AIRPRO campaign, the O₃ production regime remained
82 VOC-limited, with the exception of a few days in the afternoon when the NO mixing ratio
83 dropped low enough for the O₃ regime to shift towards NO_x-limited. The O₃ sensitivity to VOC,
84 the dominant regime during the summer AIRPRO campaign, was observed to decrease and
85 shift towards a NO_x sensitive regime both when NO mixing ratio decreased and with the
86 addition of aerosol uptake. This suggests that if [NO_x] continues to decrease in the future, ozone
87 reduction policies focussing solely on NO_x reductions may not be as efficient as expected if

88 [PM] and, hence, HO₂ uptake to aerosol surfaces, continues to decrease. The addition of aerosol
89 uptake into the model, for both the γ_{HO_2} calculated from measured data and when using a fixed
90 value of $\gamma_{HO_2} = 0.2$, did not have a significant effect on the overall O₃ production regime across
91 the campaign. While not important for this campaign, aerosol uptake could be important for
92 areas of lower NO concentration that are already in a NO_x-sensitive regime.

93 **1 Introduction**

94 Climate change and air quality are two significant environmental issues faced by society today
95 with the drive to net zero emissions by 2050 becoming increasingly important to remain
96 consistent with the long-term anthropogenic temperature warming outcome of below 1.5 °C as
97 set out by the Paris Agreement in 2016. Increasing anthropogenic emissions have caused not
98 only an increase in atmospheric warming, but also a deterioration in atmospheric air quality: a
99 concern due to both short and long term negative health effects seen as a product of poor air
100 quality such as respiratory and cardiovascular diseases and cancer (Brauer et al., 2016; Gakidou
101 et al., 2017), in addition to a variety of negative effects on the environment such as increased
102 soil acidification and the ensuing damage to vegetation and crop yield as a by-product of
103 increasing acidity of rain (Forster et al., 2007).

104 Ambient air pollution has become a serious issue globally, specifically in large urban areas
105 effected by anthropogenic emission sources. Due to rapid industrialisation, Chinese megacities
106 in particular face significant environmental and health challenges from the decline in air quality
107 following urbanisation, with areas such as the Beijing-Tianjin-Hebei area in the North China
108 Plain (NCP) suffering from seasonal extreme pollution episodes as a consequence (Wang,
109 2021; Jin et al., 2016). In terms of human health, the most important pollutants in many regions
110 are ground level O₃, NO_x (NO₂ and NO) and particulate matter. Nitrogen dioxide (NO₂) can be
111 directly emitted into the atmosphere from high temperature combustion sources or can be
112 formed via the reaction of nitrogen monoxide (NO) with an oxidising species in the
113 troposphere, such as HO₂, leading to the formation of hydroxyl radical (OH) (Ye et al., 2017).
114 Ozone, while vital in the stratosphere to protect the earth from harmful UV radiation and
115 excessive planetary heating, is toxic to both plant and human life at ground level and can react
116 with NO to form NO₂. Particulate matter is emitted anthropogenically and biogenically and can
117 play a role in the warming and cooling of the atmosphere due to the ability of aerosols to absorb
118 or scatter IR radiation depending on their composition. High levels of particulate matter, NO_x

119 and tropospheric O₃ in areas of low atmospheric mixing lead to photochemical smog and the
120 reduction of visibility characteristic of extreme pollution episodes.

121 The concentration of pollutants and trace gases in the troposphere is controlled not only by
122 emission levels but also by the oxidation capacity of the atmosphere which is determined
123 largely by the concentration of the hydroxyl radical (OH) and the closely coupled hydroperoxyl
124 (HO₂) radical, referred to collectively as HO_x radicals. Known for their role in chemical
125 oxidation processes in the atmosphere, OH and HO₂ are vital species when considering climate
126 change and air pollution. The OH radical is the main daytime tropospheric oxidant, with a
127 major role as a source of ground level ozone (O₃) (Levy, 1971) and as a sink for both
128 atmospheric pollutants, such as methane, and other radical species. The OH radical also has a
129 role in the formation of secondary pollutants including secondary organic aerosols (SOAs)
130 formed via the oxidation of volatile organic compounds (VOCs). OH and HO₂ radicals are
131 closely linked, due to the recycling of HO₂ to give OH, either via the reaction with NO or CO,
132 with the dominant loss pathway of HO₂ in polluted regions being the reaction with NO to form
133 OH (for example, as shown in Beijing by Slater et al., 2020; Whalley et al., 2021). As such,
134 understanding the sources and sinks of both OH and HO₂ within the troposphere is crucial to
135 fully understand the concentration and distribution of trace atmospheric species associated with
136 climate change and poor air quality.

137 Observed HO₂ concentrations from field measurements frequently can-not be fully explained
138 by atmospheric chemistry models which often have a tendency to over-predict HO₂ in low NO_x
139 conditions (Kanaya et al., 2007; Commane et al., 2010; Whalley et al., 2010; Whalley et al.,
140 2021; Slater et al., 2020; Sommariva et al., 2004). Following the ClearLo campaign in London
141 2012, zero-dimensional modelling showed an over-prediction of HO₂ by up to a factor of 10 at
142 low NO_x which was attributed to uncertainties in the degradation mechanism of complex
143 biogenic and diesel-related VOC species at low NO_x (Whalley et al., 2018). Over-prediction of
144 HO₂ is also commonly thought to be due, in part, to lack of understanding of HO₂ uptake onto
145 aerosol surfaces. A 2014 modelling study by Xue et al., 2014 focussing on the transport,
146 heterogeneous chemistry and precursors of ground level ozone in Beijing, Shanghai,
147 Guangzhou and Lanzhou, identified HO₂ uptake as a source of uncertainty when considering
148 ozone production, with uptake onto aerosols having the largest effect on HO₂ concentration in
149 Beijing where aerosol loadings were the highest.

150 While the impact of HO₂ uptake on HO_x concentrations has been calculated to vary from ~10-
151 40 % (Jacob, 2000; Whalley et al., 2010; Whalley et al., 2021; Slater et al., 2020; Mao et al.,
152 2010; Li et al., 2019; Li et al., 2018) globally, often a single value of $\gamma_{HO_2} = 0.2$ is used within
153 models, as recommended by Jacob, 2000. Previous experimental studies report uptake
154 coefficients which span several orders of magnitude, however, and vary largely based on the
155 state of the aerosol and whether transition metal ion catalysis is involved. For dry inorganic
156 salt aerosols values as low as $\gamma_{HO_2} < 0.002$ have been reported (Cooper and Abbatt, 1996;
157 Taketani et al., 2008; George et al., 2013) increasing to up to $\gamma_{HO_2} = 0.2$ for aqueous aerosols
158 (Thornton and Abbatt, 2005; Taketani et al., 2008; George et al., 2013). Previous experimental
159 studies report much higher $\gamma_{HO_2} > 0.4$ for Cu-doped aqueous aerosols (Thornton and Abbatt,
160 2005; Mozurkewich et al., 1987; Taketani et al., 2008; George et al., 2013; Lakey et al., 2016).
161 Recently, larger values of γ_{HO_2} have been measured experimentally from samples taken offline
162 at Mt. Tai (0.13-0.34) and Mt. Mang (0.09-0.40) in China by Taketani et al., 2012, while
163 another study in Kyoto, Japan, directly measured γ_{HO_2} values under ambient conditions from
164 0.08 to 0.36 (Zhou et al., 2020). With $\gamma_{HO_2} > 0.1$, HO₂ concentrations can be significantly
165 influenced particularly in areas of low [NO] and/or high aerosol loadings (Lakey et al., 2015;
166 Matthews et al., 2014; Mao et al., 2013; Zhou et al., 2021; Martinez et al., 2003).

167 Following multiple policies implemented across China in response to the poor air quality
168 “crisis”, a number of studies have reported a decrease in NO_x and PM_{2.5} emissions in China
169 (Jin et al., 2016). Liu et al., 2017 reported NO_x (NO₂ + NO) emissions over 48 Chinese cities
170 to have decreased by 21 % in the period of 2011-2015, supported by observed declines in NO_x
171 emissions reported by other studies (Krotkov et al., 2016; Liu et al., 2016; Miyazaki et al.,
172 2017; Van Der A et al., 2017). Ma et al., 2016b reported a mean annual decrease in PM_{2.5} of
173 0.46 $\mu\text{g m}^{-3}$ between 2008-2013, while Lin et al., 2018 reported an average decrease of 0.65
174 $\mu\text{g m}^{-3} \text{ yr}^{-1}$ between 2006-2010 increasing to a decline of 2.33 $\mu\text{g m}^{-3} \text{ yr}^{-1}$ for the period of
175 2011-2015. In contrast to the observed decrease in NO_x and PM_{2.5} emissions, several studies
176 have reported increasing O₃ levels. Ma et al., 2016a reported a maximum daily average 8h
177 mean (MDA8) increase in O₃ concentrations of 1.13 ppb yr⁻¹ for the period between 2003-2015
178 at a rural site north of Beijing while satellite observations suggested ground level ozone had
179 increased ~7% for the period between 2005-2010 (Verstraeten et al., 2015). A recent study by
180 Silver et al., 2018 also observed a significant increase in O₃ concentrations with median MDA8
181 increasing at a rate of 4.6 $\mu\text{g m}^{-3} \text{ yr}^{-1}$ across China.

182 A 2018 modelling study using the regional model GEOS-Chem by Li et al., 2018 suggested
183 the increase in O₃ across China between 2013-2017 could be attributed to the decrease in PM_{2.5},
184 with changes in PM_{2.5} being a more important driver of increasing O₃ trends than NO_x and
185 VOC emissions for the period studied. It was proposed that a decrease in PM_{2.5} emissions had
186 led to a decrease in loss of HO₂ via aerosol uptake resulting in an increase in HO₂ concentration,
187 and a proportional increase in the loss of HO₂ via NO leading to NO₂ which, when photolyzed,
188 forms O₃ leading to an increase in O₃ (Li et al., 2018). However, analysis of measured radical
189 budget from a field campaign in the North China Plain in Summer 2014 with a calculated γ_{HO_2}
190 of 0.08 ± 0.13 , showed no evidence for a significant impact of HO₂ heterogeneous chemistry
191 on radical concentrations in North China Plain, concluding that reduced HO₂ uptake was
192 unlikely to therefore be the cause of increasing O₃ levels in the North China Plain (Tan et al.,
193 2020). Using a novel parameterisation developed by Song et al., 2020 in the framework of the
194 resistor model to take into account the influence of aerosol soluble copper, aerosol liquid water
195 content and particulate matter concentration on HO₂ uptake, and the Multiphase Chemical
196 Kinetic box model (PKU-MARK) to assess the impact of HO₂ uptake on the O₃ budget for
197 Wangdu Campaign in 2014, Song et al., 2022 concluded that HO₂ heterogeneous processes
198 could decrease the O₃ production rates by up to 6 ppbv hr⁻¹, particularly in the morning VOC-
199 limited regime.

200 In this study, the new parameterisation introduced by Song et al., 2021, hereafter referred to
201 solely as the Song parameterisation, coupled with measured data from the Summer AIRPRO
202 campaign in Beijing 2017 was used to calculate a time series of the HO₂ uptake coefficient,
203 which was then used to investigate the impact of heterogeneous uptake of HO₂ onto aerosol
204 surfaces on the HO₂ radical budget in Summertime Beijing using the Master Chemical
205 Mechanism and the impact on the O₃ regime. We will test the hypothesis that reduced HO₂
206 uptake due to a reduction in PM_{2.5} concentration is a significant driver of the recent increase in
207 ozone concentrations in China.

208 **2 Experimental**

209 **2.1 Campaign overview and site description**

210 As part of the Atmospheric Pollution and Human Health (APHH) in a Chinese Megacity
211 programme, the University of Leeds took simultaneous measurements of OH, HO₂, RO₂ and
212 OH reactivity (k_{OH}), in addition to measurements of HCHO and photolysis rates, during two

213 field campaigns at an urban site in Winter 2016 and Summer 2017 in Beijing, with the aim to
214 study the chemical and physical processes governing gas and particle pollution and
215 meteorological dynamics in the Beijing region and the links between the two (Shi et al., 2019;
216 Slater et al., 2020; Whalley et al., 2021). The two field campaigns in Beijing were part of the
217 AIRPRO (The integrated study of AIR pollution PROCesses in Beijing) project within the
218 APHH programme, described fully by Shi et al., 2019.

219 For the summer AIRPRO campaign, the official science period was from 23rd May 2017 to the
220 22nd June 2017, with observations taking place at the Institute of Atmospheric Physics (IAP)
221 within the Chinese Academy of Sciences, located between the third and fourth ring roads in
222 central Beijing within 100 m of a major road, making local traffic emission sources an
223 important source of pollution during measurement period. All instrumentation for the campaign
224 was located at this site, housed within nine shipping containers surrounding a meteorological
225 tower. Further details of the instrumentation and measurement site can be found in Shi et al.,
226 2019.

227 **2.2 FAGE instrumentation description**

228 ~~The University of Leeds Fluorescence Assay by Gas Expansion (FAGE) instrument made~~
229 ~~measurements of OH, HO₂ and RO₂ radicals and OH reactivity (*k*_{OH}). The FAGE instrument~~
230 ~~set-up is described fully in Whalley et al., 2018 while the OH reactivity instrument set-up is~~
231 ~~described fully in Whalley et al., 2016. Both instruments are also described fully in Slater et~~
232 ~~al., 2020 and so only a brief description is given here.~~

233 ~~Two cells, a HO_x cell and a RO_x cell connected together with a side arm, were used to take~~
234 ~~radical measurements from the roof of the Leeds FAGE lab container. A RO_xLIF flow reactor~~
235 ~~was also coupled to the RO_x cell to allow for detection of RO₂ (total, complex and simple) as~~
236 ~~described by Fuchs et al., 2008. The HO_x cell took sequential measurements of OH and the~~
237 ~~sum of OH and HO₂, by the addition of NO (Messer, 99.5 %), which titrated HO₂ to OH for~~
238 ~~detection by Laser Induced Fluorescence (LIF) at 308 nm.~~

239 ~~The RO_xLIF reactor operated in 2 modes: a ‘HO_x mode’ where a flow of CO (10 % in N₂) was~~
240 ~~added to ambient sampled air close to the pin hole to convert all ambient OH to HO₂; and a~~
241 ~~‘RO_x mode’ where NO (500 ppmv in N₂) was added in addition to the CO flow to convert all~~
242 ~~RO₂ into OH before all OH was then rapidly converted by CO into HO₂. The air from the~~
243 ~~RO_xLIF reactor was then drawn into the FAGE low pressure fluorescence cell, whereupon pure~~

244 NO (Messer, 99.5 %) was injected to convert HO₂ to OH. In HO_x mode, the sum of OH, HO₂
245 and complex RO₂ was measured, while in RO_x mode, the sum of OH, HO₂ and total RO₂ was
246 measured. From this the concentration of complex RO₂ and HO₂/OH from RO_x can be
247 determined.

248 An Inlet Pre Injector was used attached to the HO_x cell to remove ambient OH by injecting
249 propane directly above the inlet of the cell. This leads to a background measurement while the
250 laser is still online to the OH transition; this background is known as OH_{CHEM}. OH_{CHEM} includes
251 signal from laser scatter and scattered solar radiation and any fluorescence signal from any OH
252 generated inside the cell from an interference precursor. By comparing OH_{CHEM} to the signal
253 generated when the 308 nm laser tuned off the OH transition, OH_{WAVE}, the contribution of any
254 interference can be identified. While the laser is offline, OH_{WAVE}, any signal seen is from laser
255 scattered light and scattered solar radiation. Agreement between OH_{WAVE} and OH_{CHEM} was
256 generally very good during the Summer AIRPRO campaign with an overall orthogonal
257 distance regression slope of 1.103 ± 0.017 , with the exception of an interference seen when O₃
258 levels were elevated (see Woodward-Massey et al., 2020 for details).

259 **2.32.2 Determination of aerosol soluble copper concentration through ICP-** 260 **MS Analysis**

261 The soluble copper ion concentration was determined by analysing the effluent extracted from
262 quartz filter samples taken daily for the entire campaign using Inductively Coupled Plasma
263 Mass Spectrometry (ICP-MS). A 6 cm² punch from each large quartz filter PM_{2.5} sample was
264 cut and put in a 15 mL extraction tube and extracted with 10 mL ultrapure water (18.2 MΩ
265 cm) under ultrasonication for 60 minutes at below 35 °C. The sample was then shaken by a
266 temperature-controlled shaker at 4 °C for 3 hours at approximately 60 cycles min⁻¹. After
267 filtering through a filter syringe, 8 mL of effluent was transferred to a new 15 mL metal free
268 tube, and 2 mL of 10% HNO₃ was added to make a 10 mL 2% HNO₃ extract solution which
269 was then analysed to determine the soluble copper ion concentration using ICP-MS.

270 **2.42.3 MCM v3.3.1 box model description**

271 The Master Chemical Mechanism (MCMv3.3.1) is a near-explicit mechanism which describes
272 the gas-phase degradation of a series of primary emitted VOC's in the troposphere. The
273 mechanism considers the degradation of 143 VOC's and contains ~17000 elementary reactions
274 of 6700 species (Whalley et al., 2013).

275 The model was constrained to measurements of NO, NO₂, O₃, CO, HCHO, HNO₃, HONO,
 276 PAN, H₂O vapour, temperature, pressure, $j(\text{O}^1\text{D})$, $j(\text{HONO})$, $j(\text{NO}_2)$, $j(\text{ClONO}_2)$, $j(\text{HOCl})$,
 277 $j(\text{ClONO}_2)$ and specific VOC species measured using GC-FID (gas chromatography with
 278 flame ionisation) and PTR-ToF-MS (proton-transfer reaction time of flight mass
 279 spectrometry). The measured species were input into the model at a time resolution of 15
 280 minutes, with species measured at a higher time resolution averaged up to 15 minutes and those
 281 measured at a lower time resolution interpolated to give a value every 15 minutes. The full list
 282 of all species constrained in the model is shown in [Table 1](#).

Type	Species
Gas-phase inorganic species	NO, NO ₂ , O ₃ , CO, HNO ₃ , HONO, H ₂ O, SO ₂ , ClONO ₂ , HOCl
Gas-phase organic species	HCHO, PAN, CH ₄ , C ₂ H ₆ , C ₂ H ₄ , C ₃ H ₈ , C ₃ H ₆ , isobutane, butane, C ₂ H ₂ , trans-but-2-ene, but-1-ene, Isobutene, cis-but-2-ene, 2-Methylbutane, pentane, acetone, 1,3-butadiene, trans-2-pentene, cis-2-pentene, 2-methylpentane, 3-methylpentane, hexane, isoprene, heptane, benzene, toluene, nonane, decane, undecane, dodecane, o-xylene, CH ₃ OH, CH ₃ OCH ₃ , 2-ethyltoluene, 3-ethyltoluene, 4-ethyltoluene, ethylbenzene, CH ₃ CHO, C ₂ H ₅ OH, α -pinene, limonene, isopropylbenzene, propylbenzene, m-xylene, p-xylene, 1,2,3-trimethylbenzene, 1,2,4-trimethylbenzene, 1,3,5-trimethylbenzene.
Photolysis rates	$j(\text{O}^1\text{D})$, $j(\text{HONO})$, $j(\text{NO}_2)$, $j(\text{ClONO}_2)$, $j(\text{HOCl})$, $j(\text{ClONO}_2)$
Other	Mixing height, aerosol surface area

283 **Table 1.** Full description of measured species during Summer AIRPRO campaign constrained within the model
 284 The different model scenarios referred to in this study are described in full below:

- 285 1. **MCM_base:** The base model run constrained to species described in [Table 1](#)
 286 **†**.
- 287 2. **MCM_gamma:** The base model including heterogeneous HO₂ uptake onto
 288 aerosols with γ_{HO_2} calculated from parameterisation developed by Song et al., 2020.
- 289 3. **MCM_SA:** The base model including heterogeneous HO₂ uptake, this time with
 290 γ_{HO_2} fixed at 0.2, as commonly used within models and recommended by Jacob,
 291 2000.

Formatted: Font: 12 pt, Not Bold

Formatted: Font: 12 pt, Not Bold, Not Italic

Formatted: Font: 12 pt, Not Bold

Formatted: Font: 12 pt, Not Bold, Not Italic

2.4 Calculation of L_N/Q and absolute O_3 sensitivity

First introduced by Kleinman et al., 1997, L_N/Q is the ratio of radical loss via NO_x to total primary radical production and is used as a means of determining O_3 production sensitivity to VOCs and NO_x (Kleinman, 2000; Kleinman et al., 1997; Kleinman et al., 2001). This method was then built on by Sakamoto et al., 2019 who included loss of peroxy radicals ($XO_2=HO_2+RO_2$) onto aerosol surfaces within the calculation of O_3 sensitivity.

The only source of tropospheric O_3 is by the reaction of peroxy radicals with NO , while the main source of XO_2 species is via the reaction of OH with VOCs.



The O_3 production rate in the troposphere is therefore:

$$P(O_3) = k_{HO_2+NO}[HO_2][NO] + k_{RO_2+NO}[RO_2][NO] \quad (21)$$

where k_{HO_2+NO} and k_{RO_2+NO} are the bimolecular rate constants for the reaction of HO_2 and RO_2 with NO .

The production rate of OH , HO_2 and RO_2 radicals, Q , must equal the loss rate:

$$Q = L_P + L_N + L_R \quad (32)$$

where L_P is the loss rate of radicals onto aerosol particles, L_N is the loss rate of radicals via reaction with NO_x species and L_R is the loss rate of radicals via radical-radical reactions to give peroxides.

$$L_P = k_{HO_2 \text{ uptake}}[HO_2] + k_{RO_2 \text{ uptake}}[RO_2] = k_P[XO_2] \quad (34)$$

$$L_N \approx k_{NO_2+OH}[NO_2][OH] \quad (45)$$

$$L_R = 2(k_{HO_2+HO_2}[HO_2]^2 + k_{RO_2+HO_2}[HO_2][RO_2]) \quad (56)$$

where $k_{HO_2 \text{ uptake}}$ is the rate constant for the loss of HO_2 onto aerosol surfaces, $k_{RO_2 \text{ uptake}}$ is the rate constant for the loss of RO_2 onto aerosol surfaces, k_{NO_2+OH} is the bimolecular rate constant for the reaction of NO_2 with OH , $k_{HO_2+HO_2}$ is the bimolecular rate constant for the self-reaction of HO_2 and $k_{RO_2+HO_2}$ is the bimolecular rate constant for the reaction of RO_2 with HO_2 .

Formatted: Heading 2, Left

312 For radical loss onto aerosol surfaces, the rate constant is given as a function of the reactive
 313 uptake coefficient, γ_{XO_2} , aerosol particle surface area ($\text{cm}^2 \text{cm}^{-3}$) and mean thermal velocity
 314 (cm s^{-1}), given by $v = \sqrt{8RT/\pi M}$ with R, T and M as the gas constant, the absolute temperature
 315 and the molar mass of species respectively.

$$k_{\text{radical uptake}} = \frac{\gamma_{XO_2} \times SA \times v}{4} \quad (67)$$

316 According to the method described in Sakamoto et al., 2019, the ratio of radical loss to NO_x to
 317 primary O_3 production including radical loss via aerosol uptake, $\frac{L_N}{Q}$ is defined as follows:

$$\frac{L_N}{Q} = \frac{1}{1 + \left(\frac{(2k_R[XO_2] + k_P)k_{OH+VOC}[VOC]}{(1-\alpha)k_{HO_2+NO}[NO]k_{NO_2+OH}[NO_2]} \right)} \quad (78)$$

318 where k_{OH+VOC} is the bimolecular rate constant for the loss of OH via reaction with VOCs and
 319 $(1-\alpha)$ is the fraction of XO_2 that is HO_2 .

320 The relative sensitivity of O_3 production to NO_x and VOCs is described by:

$$\frac{\delta \ln P(O_3)}{\delta \ln [NO_x]} = (1-\chi) \left(\frac{1 - \frac{3L_N}{2Q}}{1 - \frac{1L_N}{2Q}} \right) + \chi \left(1 - 2\frac{L_N}{Q} \right) \quad (89)$$

$$\frac{\delta \ln P(O_3)}{\delta \ln [VOC]} = (1-\chi) \left(\frac{\frac{1L_N}{2Q}}{1 - \frac{1L_N}{2Q}} \right) + \chi \frac{L_N}{Q} \quad (910)$$

321 where $\chi = \frac{L_P}{L_P+L_R}$. The O_3 regime transition point, where $\frac{\delta \ln P(O_3)}{\delta \ln [NO_x]} = \frac{\delta \ln P(O_3)}{\delta \ln [VOC]}$ is given by $\frac{L_N}{Q_{\text{trans}}}$.

$$\frac{L_N}{Q_{\text{trans}}} = \frac{1}{2}(1-\chi) + \frac{1}{3}\chi \quad (101)$$

322 Absolute O_3 sensitivity was introduced by Sakamoto et al., 2019, and allows for the assessment
 323 of how reduction in O_3 precursors could contribute to reduction in $P(\text{O}_3)$ by integrating over
 324 time and area. The absolute sensitivity of O_3 production to VOC and NO_x is then described by:

$$\text{Absolute } P(O_3) = \frac{\delta P(O_3)}{\delta \ln [X]} = P(O_3) \frac{\delta P(O_3)}{\delta \ln [X]} \quad (112)$$

325 where is $[X]$ is NO_x or VOC.

2.5

2.5.2.6 Description of the “Song parameterisation”

A large uncertainty in determining the effect of HO₂ uptake onto the surface of aerosol particles is the lack of understanding of the dependence of γ_{HO_2} on Cu (II)/transition metal ion concentration within aerosols. Experimentally this dependence is quite well known from laboratory studies (Mozurkewich et al., 1987; Thornton and Abbatt, 2005; George et al., 2013; Mao et al., 2013), however the effective concentrations in ambient aerosols and the impact on γ_{HO_2} of aerosol liquid water concentration, [ALWC], has not been incorporated into models before. A novel parameterisation was developed by Song et al., 2020 in the framework of the resistor model to include the influence of aerosol soluble copper on the uptake of HO₂. The new parameterisation for the uptake coefficient of HO₂ onto aerosols, as given in Song et al., 2020, is as follows:

$$\frac{1}{\gamma_{HO_2}} = \frac{1}{\alpha_{HO_2}} + \frac{3 \times v_{HO_2}}{(4 \times 10^6) \times R_d H_{eff} RT \times \left(5.87 + 3.2 \ln \left(\frac{ALWC}{[PM] + 0.067} \right) \right) \times [PM]^{-0.2} \times [Cu^{2+}]_{eff}^{0.65}} \quad (+2)$$

where γ_{HO_2} is the uptake coefficient of HO₂ onto aerosols, α_{HO_2} is the mass accommodation coefficient of HO₂, v_{HO_2} is the mean molecular speed in cm s⁻¹, R_d is the count median radius of the aerosol in cm, H_{eff} is the effective Henry’s Law constant calculated from $H_{eff} = H_{HO_2} \left(1 + \frac{K_{eq}}{[H^+]} \right)$ where H_{HO_2} is the physical Henry’s Law constant for HO₂ (i.e. 3900 (Thornton et al., 2008)) in M atm⁻¹, K_{eq} is the equilibrium constant for HO₂ dissociation (M), and $[H^+]$ is the hydrogen ion concentration within the aerosol calculated from the pH (M), R is the gas constant in cm³ atm K⁻¹ mol⁻¹ (i.e. 82.05), T is the temperature in K, [ALWC] is the aerosol liquid water content in $\mu\text{g m}^{-3}$ (which is related to the ambient relative humidity), [PM] is the mass concentration of PM_{2.5} in $\mu\text{g m}^{-3}$ and $[Cu^{2+}]_{eff}$ is the effective aerosol condensed-phase soluble copper (II) ion concentration in mol L⁻¹.

The Song parameterisation can reportedly be used for urban environmental conditions of aerosol mass concentrations between 10-300 $\mu\text{g m}^{-3}$; aqueous copper (II) concentrations of 10⁻⁵–1 mol L⁻¹; and relative humidity between 40-90 %. However, for the Summer AIRPRO campaign data, the minimum [ALWC] supported by the parameterisation was 14 $\mu\text{g m}^{-3}$, below which the parameterisation returned negative values for γ_{HO_2} . As such, despite the average

353 calculated [ALWC] for the campaign being $6.9 \pm 10 \mu\text{g m}^{-3}$, a fixed value of $14 \mu\text{g m}^{-3}$ was
354 used to calculate γ_{HO_2} across the entire campaign.

355 **3 Results and Discussion**

356 **3.1 Overview of field observations during summer AIRPRO campaign**

357 Radical concentration measurements were taken throughout the official science period of the
358 summer campaign, from 23/05/2017 to 22/06/2017, using the Fluorescence Assay by Gas
359 Expansion technique. Alongside the radical observations and photolysis rate measurements
360 made by the University of Leeds, there was a varied suite of supporting measurements operated
361 by several universities and institutions. The supporting measurements used for the analysis and
362 discussion in this study were provided chiefly by the Universities of York, Birmingham and
363 Cambridge as detailed in [Table 2](#)~~Table 2~~.

Formatted: Font: 12 pt, Not Bold

Formatted: Font: 12 pt, Not Bold, Not Italic

364

365

366

367

368

369

370

371

372

373

374

375

376

377

378

Instrument	Species measured	University	Reference
FAGE	OH, HO ₂ , RO ₂	Leeds	Whalley et al., 2010; Whalley et al., 2021; Slater et al., 2020
OH reactivity	OH reactivity	Leeds	Stone et al., 2016; Whalley et al., 2021; Slater et al., 2020
Spectral Radiometer	Photolysis rates	Leeds	Bohn et al., 2016
Filter Radiometer	$j(\text{O}^1\text{D})$	Leeds	Whalley et al., 2010
Teledyne CAPS	NO ₂	York	Smith et al., 2017
TEI 42c	Total NO _y	York	Smith et al., 2017
TEI 49i	O ₃	York	Smith et al., 2017
Sensor box	CO	York	Smith et al., 2017
DC-GC_FID	C ₂ -C ₇ VOCs and oVOCs	York	Hopkins et al., 2011
GCxGC-FID	C ₆ -C ₁₃ VOCs and oVOCs	York	Dunmore et al., 2015
BBCEAS	HONO	Cambridge	Le Breton et al., 2014
TEI 42i	NO	Birmingham	-
LOPAP	HONO	Birmingham	Crilley et al., 2016
SMPS	Particle Size distribution	Birmingham	Wiedensohler et al., 2012
High volume sampler	PM _{2.5} filter samples, Aerosol copper	IAP	-

380 **Table 2.** Measurements taken by universities and institutions during the Beijing Summer AIRPRO campaign.
381 These species are directly referred to in this chapter: full description of every instrument and measurement taken
382 can be found in Slater, 2020. IAP: Institute of Atmospheric Physics, Beijing. Time resolution of all instruments
383 was averaged up to or interpolated down to 15 minutes for modelling purposes with the exception of the PM_{2.5}
384 filter samples, of which there was only 1 sample taken a day.

385 The median average diurnals for important gas phase species (ppb) and $j(\text{O}^1\text{D})$ (s⁻¹) measured
386 during the summer campaign are shown in ~~Figure 1~~ **Figure 4**. $j(\text{O}^1\text{D})$ showed a maximum at
387 solar noon peaking at 2.5×10^{-5} s⁻¹. The diurnal variation in both NO and NO₂ was very
388 distinct, with a peak in NO at rush hour (~08:00) of ~ 8 ppb. NO decreased into the afternoon
389 following this morning peak to a minimum of 0.3 ppb. The low values of NO mixing ratio
390 observed in the afternoon were a result of high levels of O₃, peaking at 89 ppb at ~15:30,
391 leading to increased titration of NO + O₃ to give NO₂, the diurnal of which can be seen to peak
392 in the morning at ~ 32 ppb at 06:30, coinciding with peak in traffic emissions. Conversely

Formatted: Font: 12 pt, Not Bold

Formatted: Font: 12 pt, Not Bold, Not Italic

393 O₃ mixing ratio was at a minimum of ~14 ppb during the morning traffic peak in NO. Due to
 394 the expected accumulation of HONO overnight, HONO mixing ratio is highest in the morning,
 395 peaking before 07:30 at ~7 ppb, after which HONO is lost rapidly via photolysis to give OH
 396 + NO. This study will use these measured observations to compare modelled and measured
 397 concentrations of OH, HO₂ and RO₂ radicals and investigate the effect of HO₂ uptake on radical
 398 concentrations.

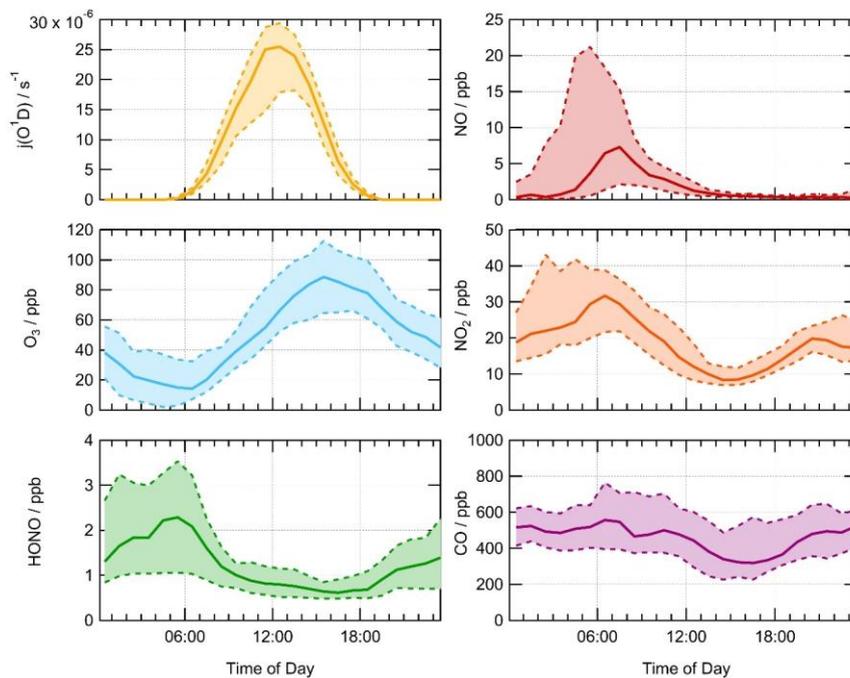


Figure 1. Average median diurnal profile for measured $j(\text{O}^1\text{D})$ (s^{-1}), O₃ (ppb), HONO (ppb), NO (ppb), NO₂ (ppb) and CO (ppb) for the Summer AIRPRO campaign. The dashed lines with shaded regions represent the 25th/75th percentiles. Diurnals show 60 minute averages, taken over the entire measurement period.

399 The majority of the Summer Beijing campaign occurred during a non-haze period, meaning
 400 PM_{2.5} concentrations remained below 75 $\mu\text{g m}^{-3}$, only exceeding this on the 28/05, 31/05,
 401 05/06, 07/06, 17/06 and 18/06/2017. The average median diurnal of PM_{2.5} surface area
 402 ($\text{cm}^2 \text{cm}^{-3}$) is shown in [Figure 2](#). PM_{2.5} surface area concentration was available at a
 403 higher resolution due to use of online particle sizers compared to filter samples taken daily to
 404 give PM_{2.5} mass concentration. PM_{2.5} surface area was then averaged up to a time resolution
 405 of 15 minutes to be used in the model. [Online particle sizers were run without a drying inlet to](#)

Formatted: Font: 12 pt, Not Bold

Formatted: Font: 12 pt, Not Bold, Not Italic

406 ensure aerosol measurements were as close to real ambient size distributions as possible, and
407 therefore correction for hygroscopic growth was not necessary. No strong diurnal trend was
408 seen, with an average across the campaign of $5.5 \times 10^{-6} \text{ cm}^2 \text{ cm}^{-3}$, with a maximum surface
409 area of $2.5 \times 10^{-5} \text{ cm}^2 \text{ cm}^{-3}$.

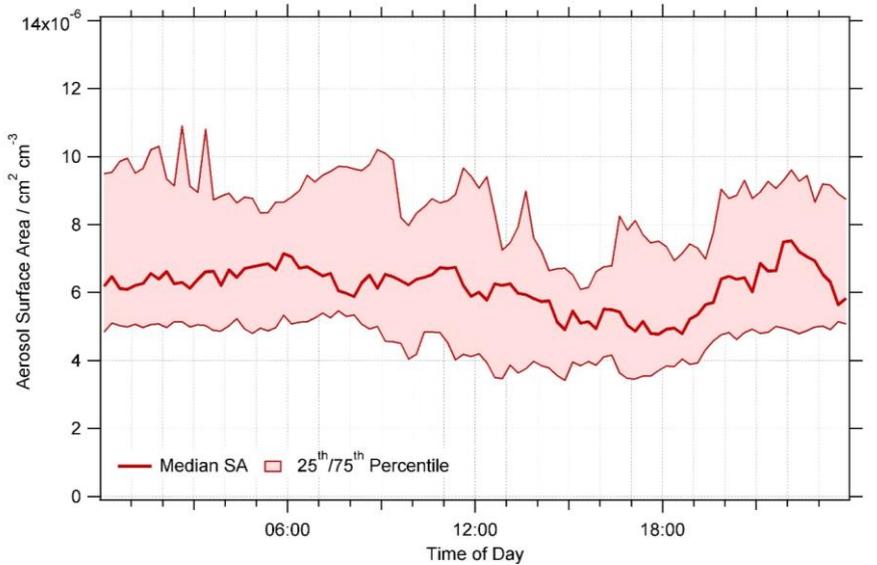


Figure 2. Average median diurnal of $\text{PM}_{2.5}$ aerosol surface area ($\text{cm}^2 \text{ cm}^{-3}$) for Summer AIRPRO campaign. Data averaged up to 15 mins time resolution. The dashed lines with shaded regions represent the 25th/75th percentiles.

410 During haze periods in Beijing, it is expected that a strong correlation would exist between
411 $\text{PM}_{2.5}$ and NO_x , as seen in Winter Beijing AIRPRO campaign in 2016 (Slater et al., 2020).
412 However, during the Summer campaign, no strong correlation between $\text{PM}_{2.5}$ and NO_x was
413 seen. The time series of NO (ppb) and $\text{PM}_{2.5}$ ($\text{cm}^2 \text{ cm}^{-3}$) is shown in [Figure 3](#). A
414 correlation plot of $\text{PM}_{2.5}$ aerosol surface area ($\text{cm}^2 \text{ cm}^{-3}$) versus NO and NO_2 mixing ratio (ppb)
415 is shown in Figure 1 of Supplementary Information.

Formatted: Font: 12 pt, Not Bold

Formatted: Font: 12 pt, Not Bold, Not Italic

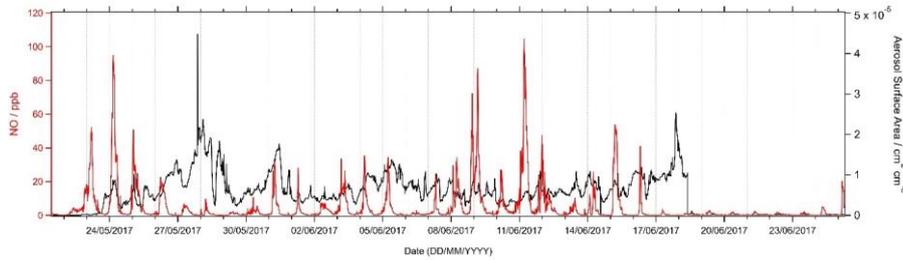


Figure 3. Time series of measured NO / ppb and PM_{2.5} / cm² cm⁻³ across entire summer AIRPRO campaign in Beijing.

416 3.2 Calculated γ_{HO_2} for summer AIRPRO campaign

417 Measured values of [PM], copper (II) ion concentration and aerosol pH (used to calculate H_{eff}
 418 in equation 12), and values of [ALWC] estimated using the ISORROPIA-II thermodynamic
 419 equilibrium model (Fountoukis and Nenes, 2007) were input into the parameterisation at a time
 420 resolution of 1 day. PM_{2.5} mass concentration and Cu (II) ion concentration values were
 421 measured by extracting from filter samples offline with one filter sample taken every day. As
 422 such all measured values input into the parameterisation were averaged up to this time
 423 resolution. R_d was calculated from the measured aerosol size distribution across the entire
 424 campaign. A value of 0.5 was chosen for the mass accommodation coefficient, α_{HO_2} , to reflect
 425 values previously measured for copper doped inorganic salts (Thornton and Abbatt, 2005;
 426 George et al., 2013; Taketani et al., 2008) and to allow better comparison with results from
 427 Song et al., 2020. For summer AIRPRO campaign, the soluble copper ion concentration was
 428 measured by extracting Cu (II) ions from filter samples and analysing the effluent using
 429 Inductively Coupled Plasma Mass Spectrometry (ICP-MS). As in Song et al., 2020, the total
 430 copper (II) mass concentration (ng m⁻³ converted to g m⁻³) was divided by the aerosol volume
 431 concentration (nm³ cm⁻³ converted to dm³ m⁻³) and the molar mass of copper (g mol⁻¹) to give
 432 the total copper molar concentration in the aerosol, $[Cu^{2+}]_{eff}$ (mol L⁻¹), which was then used in
 433 equation 12. The average values across summer AIRPRO campaign for parameters used in
 434 equation 12 are shown in [Table 3](#).

Parameter	Average value across campaign
Temperature (K)	300
Relative humidity (%)	43
Aerosol pH	3

Formatted: Font: 12 pt, Not Bold

Formatted: Font: 12 pt, Not Bold, Not Italic

Count median radius (cm)	2.3×10^{-6}
ALWC ($\mu\text{g m}^{-3}$)^a	14
[PM] ($\mu\text{g m}^{-3}$)	38.3
[Cu²⁺]_{eff} (mol L⁻¹)	0.0008
[Cu²⁺]_{eff} (ng m⁻³)	4
a_{HO_2}	0.5 (fixed)

435 **Table 3.** Average values for summer AIRPRO campaign in Beijing, 2017 for parameters in equation 12. ^aThis
436 was a fixed minimum value of ALWC for the parameterisation to be used for this data set, fully explained in
437 Section 3.4. Cu (II) ion concentration is given in both mol L⁻¹ and ng m⁻³, due to mol L⁻¹ being used in equation
438 12 but ng m⁻³ being the more atmospherically relevant unit.

439 For the Beijing summer AIRPRO campaign, an average value of $\gamma_{HO_2} = 0.07 \pm 0.035$ (1 σ) was
440 calculated across the entire campaign, with values ranging from 0.002 to 0.15. The time series
441 for the calculated γ_{HO_2} , R_d (cm), [PM] ($\mu\text{g m}^{-3}$), [ALWC] ($\mu\text{g m}^{-3}$) and [Cu²⁺]_{eff} (mol L⁻¹) is
442 shown in [Figure 4](#).

443 As fully described in Song et al., 2020 supplementary information, the uncertainty in the
444 calculation of γ_{HO_2} using equation 12 comes mainly from the uncertainty in [ALWC] (~10-20
445 %, calculated using ISORROPIA-II (Fountoukis and Nenes, 2007)), the uncertainty in the mass
446 accommodation coefficient (varying a_{HO_2} within the parameterisation from 0.1 to 1, increased
447 the calculated γ_{HO_2} from 0.042 to 0.077. However, by $a_{HO_2} = 0.5$ this dependence has begun to
448 plateau with $\gamma_{HO_2} = 0.070$ when $a_{HO_2} = 0.5$), and the uncertainty of the model calculations used
449 to formulate the parameterisation (~40 % as explained in Song et al., 2020). Uncertainties in
450 measured parameters i.e. temperature, [PM], [Cu²⁺] and count median radius are due to
451 associated instrumental error which are assumed small in comparison.

Formatted: Font: 12 pt, Not Bold

Formatted: Font: 12 pt, Not Bold, Not Italic

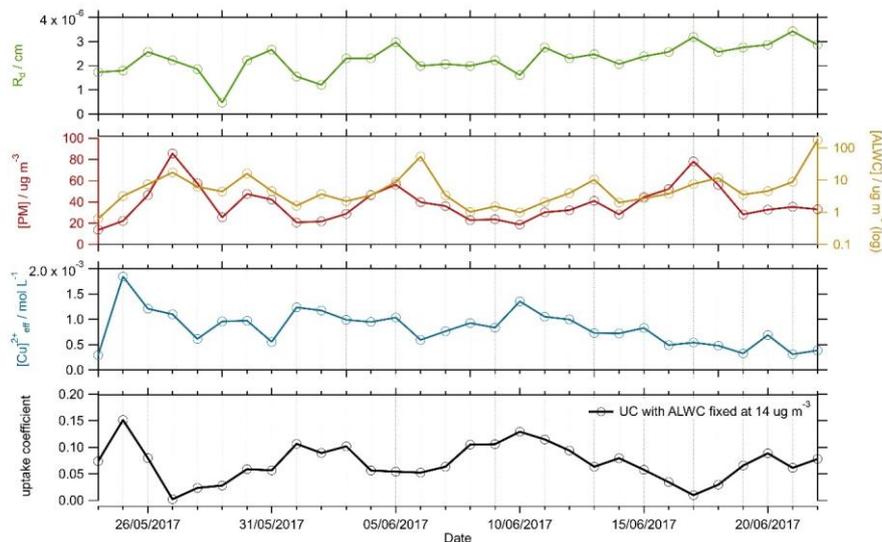


Figure 4. Time series of R_d (cm, orange), [PM] ($\mu\text{g m}^{-3}$, red), [ALWC] ($\mu\text{g m}^{-3}$, yellow) and $[\text{Cu}^{2+}]_{\text{eff}}$ (mol L^{-1} , blue), parameters used in equation 12 to calculate γ_{HO_2} (bottom panel). Each parameter has been averaged up to a time resolution of 1 day to match the lowest resolution measurement. The calculated γ_{HO_2} is shown in the bottom panel, for a fixed [ALWC] = $14 \mu\text{g m}^{-3}$ (solid black line).

452 To examine the effect within the Song parameterisation of [PM] and [ALWC] on γ_{HO_2} as a
 453 function of copper molarity, the uptake coefficient was calculated by varying the $[\text{Cu}^{2+}]_{\text{eff}}$
 454 concentration within the parameterisation with alternatively fixed values of [PM] or [ALWC].
 455 For a given value of $[\text{Cu}^{2+}]_{\text{eff}}$, at fixed [ALWC] an increase in [PM] causes a decrease in the
 456 curvature of γ_{HO_2} vs $[\text{Cu}^{2+}]_{\text{eff}}$, whereas at a fixed [PM], an increase in [ALWC] leads to an
 457 increase in γ_{HO_2} for a given $[\text{Cu}^{2+}]_{\text{eff}}$. As shown in [Figure 5](#), [ALWC] and [PM] have
 458 the greatest effect on γ_{HO_2} between $[\text{Cu}^{2+}]_{\text{eff}} = 10^{-5} - 10^{-1} \text{M}$ before the curve levels off towards
 459 the mass accommodation coefficient of 0.5, as input into the model. For context within the
 460 Beijing campaign, the curve of γ_{HO_2} vs $[\text{Cu}^{2+}]_{\text{eff}}$ was plotted in [Figure 5](#) using the
 461 average values for the AIRPRO summer campaign fixed at [ALWC] = $14 \mu\text{g m}^{-3}$ and [PM] =
 462 $38.3 \mu\text{g m}^{-3}$. For the average AIRPRO summer campaign values, an increase $[\text{Cu}^{2+}]_{\text{eff}}$ has the
 463 most effect on γ_{HO_2} between $[\text{Cu}^{2+}]_{\text{eff}} \sim 10^{-3} - 10^{-1} \text{M}$, with the average $[\text{Cu}^{2+}]_{\text{eff}}$ for the campaign
 464 being $8 \times 10^{-4} \text{M}$ (values ranged from 3×10^{-4} to $2 \times 10^{-3} \text{M}$ across campaign).

465

466

Formatted: Font: 12 pt, Not Bold

Formatted: Font: 12 pt, Not Bold, Not Italic

Formatted: Font: 12 pt, Not Bold

Formatted: Font: 12 pt, Not Bold, Not Italic

467
 468
 469
 470
 471

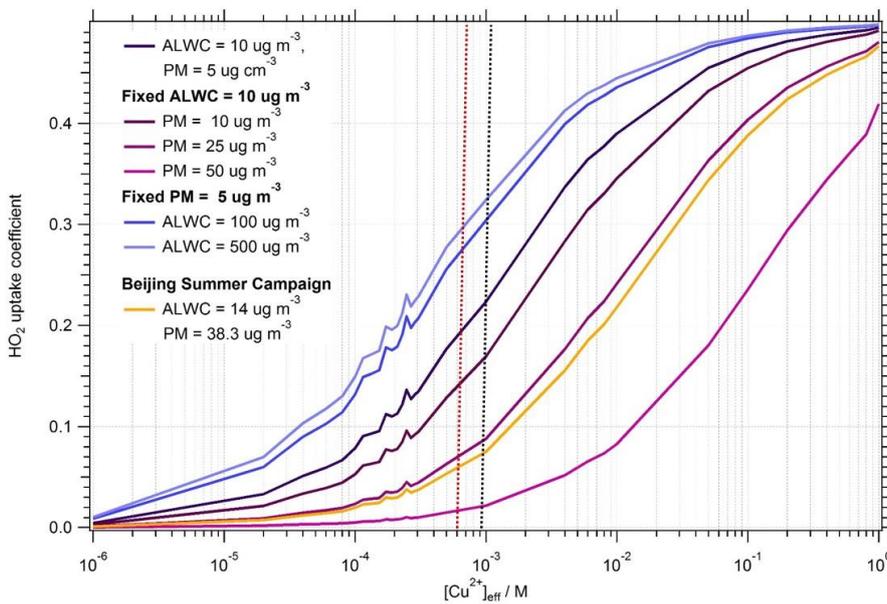


Figure 5. Dependence of uptake coefficient, γ_{HO_2} on aerosol copper concentration, $[Cu^{2+}]_{eff}$ (M), showing the effect of varying [PM] with fixed [ALWC] and vice versa. Pink to purple lines show the effect on uptake coefficient of varying [PM] from 5-50 $\mu g m^{-3}$ with a fixed [ALWC] of 10 $\mu g m^{-3}$. Blue to dark blue lines show the effect on γ_{HO_2} of varying [ALWC] from 10-500 $\mu g m^{-3}$ (much higher than typically seen atmospherically) with a fixed [PM] of 5 $\mu g m^{-3}$. The yellow line shows the effect on the γ_{HO_2} of varying $[Cu^{2+}]_{eff}$, with [ALWC] and [PM] taken as the averages from the Beijing campaign, i.e. [ALWC] = 14 $\mu g m^{-3}$ and [PM] = 38.8 $\mu g m^{-3}$. Black dashed line indicates the average $[Cu^{2+}]_{eff}$ for Beijing summer campaign. Red dashed line indicates the average $[Cu^{2+}]_{eff}$ for the Wangdu campaign. Note that the [PM] and [ALWC] are both higher for Wangdu campaign compared to the Beijing campaign.

472 3.3 Box modelling results

473 3.3.1 Effect of calculated γ_{HO_2} on modelled AIRPRO Summer radical concentrations

474 As reported in Whalley et al., 2021, radical concentrations were high during the AIRPRO
475 summer campaign with maximum measured concentrations of OH, HO₂ and RO₂ of 2.8×10^7
476 molecule cm⁻³, 1×10^9 molecule cm⁻³ and 5.5×10^9 molecule cm⁻³ on the afternoons of the
477 30th May, 9th June and 15th June respectively. The time series of measured OH, HO₂ and RO₂
478 for the entire summer campaign as measured by the Leeds FAGE instrument with MCM_base
479 model outputs for OH, HO₂ and RO₂ can be found in Whalley et al., 2021. Using the MCM
480 and the γ_{HO_2} calculated for the Summer Beijing campaign with the Song parameterisation, the
481 effect of HO₂ uptake on the concentration of OH, HO₂ and RO₂ radicals was investigated and
482 compared to the base model.

483 The MCM_base model predicted radical concentrations are shown as average diurnal profiles
484 compared to both the measured diurnals and the MCM_gamma model in [Figure 6](#). A
485 detailed description of the diurnal variation in measured and modelled OH, HO₂ and RO₂
486 radicals for the summer Beijing campaign is given in Whalley et al., 2021, so only a brief
487 summary will be given here.

488 The average diurnal profiles show that the MCM_base model can re-produce the measured OH
489 concentrations relatively well, however the modelled peak in OH is shifted to the afternoon
490 with a peak at ~14:00 compared to the midday peak in the observations. In comparison, HO₂
491 is over-predicted, particularly during the day with the exception being when NO was high from
492 9-12th June. Day-time HO₂ is over-predicted on average by MCM_base by up to a factor of
493 ~2.9 with a peak in the diurnal at ~ 14:30. In-comparison, daytime RO₂ concentration is under-
494 predicted on average by MCM_base by up to a factor of ~7.5, with a larger under-prediction
495 in the morning between ~6:30-10:30 when NO levels were highest. At the peak of the RO₂
496 diurnal, on average the concentration was under-predicted by MCM_base by a factor of ~2.7.
497 While the MCM_base model is able to reproduce measured OH concentrations reasonably
498 well, the inability of this model to reproduce HO₂ and RO₂ suggests missing key reactions. In
499 Whalley et al., 2021, budget analysis highlighted a missing source of OH, in addition to a
500 missing RO₂ production reaction which could partially explain the under-prediction of RO₂ by
501 the MCM_base model. It was also suggested that ~~the over-prediction of HO₂ could be due, in~~
502 ~~part, to an under-prediction in the rate of reaction of RO₂ with NO to produce a different RO₂~~
503 ~~species, i.e. $RO_2 + NO \rightarrow RO_2'$, which would lead to propagation of RO₂ to different, more~~

Formatted: Font: 12 pt, Not Bold

Formatted: Font: 12 pt, Not Bold, Not Italic

504 oxidised RO₂ species, competing with the recycling of RO₂ via RO to give HO₂, or due to lack
505 of RO₂ autoxidation pathways within the model which could lead to the formation of highly
506 oxygenated molecules as opposed to HO₂. The higher measured RO₂ concentrations could,
507 therefore, suggest that the lifetime of total RO₂ is longer than currently considered in the model.
508 the over-prediction of HO₂ could be due, in part, to the propagation rate of RO₂ to HO₂ being
509 significantly slower than currently included in the model. This could be due to a lack of
510 understanding of the rate of reaction of RO₂ with NO to produce different RO₂ species, i.e.
511 RO₂ + NO → RO₂', which would lead to propagation of RO₂ to different, more oxidised RO₂
512 species, competing with the recycling of RO₂ via RO₂ to give HO₂. It is also possible, that the
513 overestimation in the propagation rate of RO₂ to HO₂ could be due to a lack of RO₂ autoxidation
514 pathways included within the model which could lead to the formation of highly oxygenated
515 molecules as opposed to HO₂. The higher, measured RO₂ concentrations could, therefore,
516 suggest that the lifetime of total RO₂ is longer than currently considered within the model.

517 As stated in Section 3.3, for the Beijing summer AIRPRO campaign, values of calculated γ_{HO_2}
518 varied ranging from 0.002 to 0.15, giving an average value of $\gamma_{HO_2} = 0.07 \pm 0.035$ (1 σ) across
519 the campaign. These γ_{HO_2} values calculated on a daily time resolution, were added into the
520 MCM_base model to give the MCM_gamma model. The average median diurnals of modelled
521 OH, HO₂ and RO₂ (molecule cm⁻³) for MCM_base, MCM_gamma (with γ_{HO_2} ranging from
522 0.002-0.15) and MCM_SA (with γ_{HO_2} fixed at 0.2) are shown in [Figure 6](#) ~~Figure 6~~.

Formatted: Subscript

Formatted: Subscript

Formatted: Subscript

Formatted: Subscript

Formatted: Subscript

Formatted: Subscript

Formatted: Subscript

Formatted: Subscript

Formatted: Subscript

Formatted: Subscript

Formatted: Subscript

Formatted: Subscript

Formatted: Subscript

Formatted: Subscript

Formatted: Subscript

Formatted: Subscript

Formatted: Subscript

Formatted: Subscript

Formatted: Subscript

Formatted: Font: 12 pt, Not Bold

Formatted: Font: 12 pt, Not Bold, Not Italic

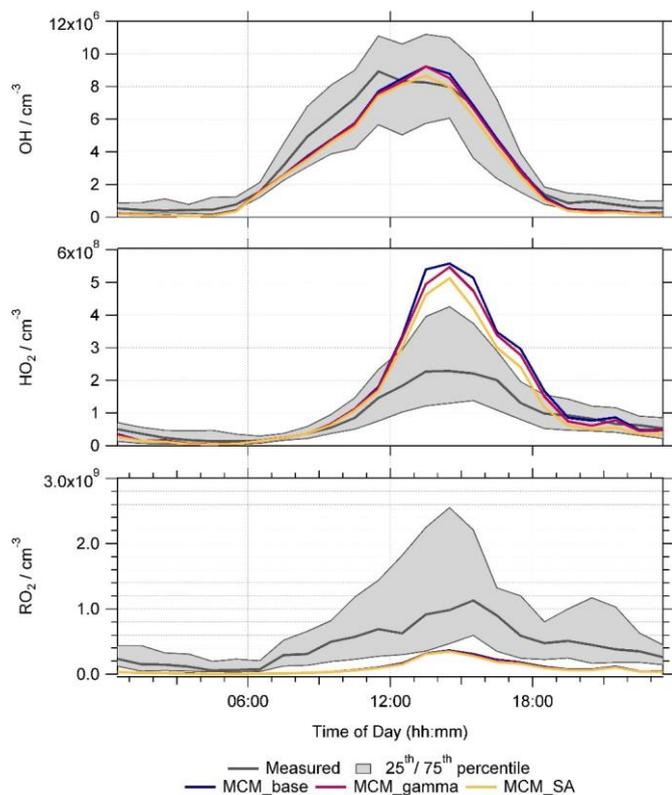


Figure 6. Average median diurnals for measured radical concentrations (grey) and modelled OH, HO₂ and total RO₂ radical concentrations in molecule cm⁻³ for MCM_base (blue), MCM_gamma (dark pink) and MCM_SA (yellow) model runs. All diurnal's are 60 minute averages, taken over the entire measurement period. Shaded grey regions represent the 25th/75th percentiles of measured radical data.

523 Due to a combination of the calculated uptake coefficient being smaller, on average, than
 524 usually used within models (i.e < 0.2), and the high NO_x levels, little effect on average radical
 525 diurnals was seen by adding in HO₂ aerosol uptake into the model. ~~Figure 6~~ **Figure 6** shows that
 526 the OH and RO₂ radical concentrations were not significantly affected on average across the
 527 campaign by the addition of aerosol uptake. The average median diurnal of HO₂ can be seen
 528 as slightly decreased, i.e. the over-prediction of HO₂ is slightly less for MCM_gamma
 529 compared to MCM_base, with the over-prediction decreasing from a factor of ~2.9 to ~2.4 at
 530 the 14:30 peak in the diurnal.

531 Due to the recycling of RO₂ to HO₂ and then back to OH by NO, it is important to consider the
 532 dependency of radicals on NO and whether the addition of the HO₂ uptake coefficient has an

Formatted: Font: 12 pt, Not Bold
 Formatted: Font: 12 pt, Not Bold, Not Italic

533 effect on the model's ability to predict the dependency of radical concentrations on NO. The
 534 dependency of measured/modelled OH, HO₂ and RO₂ on NO mixing ratio is discussed fully
 535 for the MCM_base model in Whalley et al., 2021, and is compared to MCM_gamma in Figure
 536 2 of Supplementary Information. Figure 7 shows the ratio of measured to modelled OH, HO₂
 537 and RO₂ radical concentrations binned against NO mixing ratio (ppb) for MCM_gamma,
 538 compared to MCM_base.

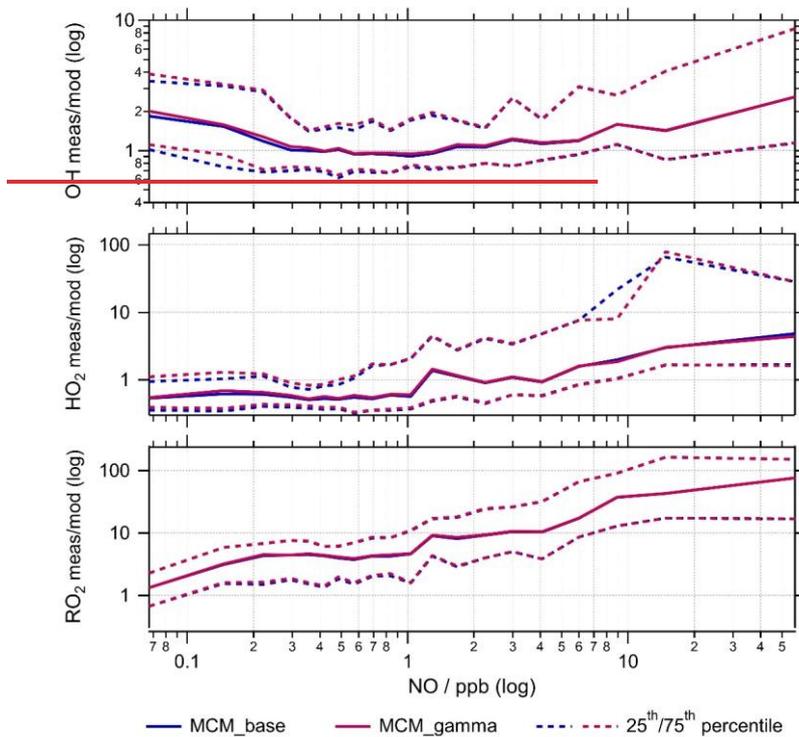


Figure 7. Ratio of measured to modelled OH, HO₂ and RO₂ radical concentrations using the MCM_base (blue) and MCM_gamma (dark pink) model binned over the range of NO mixing ratios (ppb) for the summer AIRPRO campaign. Solid lines show the median average measured to modelled radical concentration. Dashed lines show the 25th/75th percentiles.

539 For the range of NO mixing ratios observed across the summer AIRPRO campaign, the OH
 540 measured to modelled ratio is close to 1 between 0.3 and 2 ppb NO with the MCM_base
 541 model beginning to under predict OH slightly both below 0.3 ppb NO and above 2 ppb NO.
 542 Both HO₂ and RO₂ radical concentrations were strongly dependent on NO mixing ratio, with
 543 the model over predicting HO₂ below 1 ppb NO. For the entire campaign the average NO

544 ~~was 4.7 ppb with 45% of NO measurements taken across campaign being less than or equal to~~
545 ~~1 ppb. Across all NO mixing ratios the measured to modelled ratio for RO₂ shows a large~~
546 ~~under prediction, with the largest under prediction at the highest NO mixing ratios. This is~~
547 ~~likely contributing to the underprediction of HO₂ at higher NO mixing ratios. From Figure 7 it~~
548 ~~can be seen that the addition of the calculated HO₂ uptake coefficient has had little effect across~~
549 ~~the range of NO mixing ratios measured during the summer AIRPRO campaign.~~

550 To showcase any effect adding HO₂ aerosol uptake would have on HO₂ loss pathways as a
551 whole, and thereby make a judgement on the effect of decreased PM_{2.5} and hence HO₂ loss via
552 aerosol surfaces on the O₃ production within Beijing, a rate of destruction analysis (RODA)
553 was done for MCM_gamma. The loss pathways of HO₂ within MCM_gamma are shown in
554 ~~Figure 7~~ Figure 8 as an average median diurnal and as a function of NO mixing ratio (ppb), in
555 addition to the percentage contribution of HO₂ uptake to the overall loss of HO₂ within the
556 model.

Formatted: Font: 12 pt, Not Bold

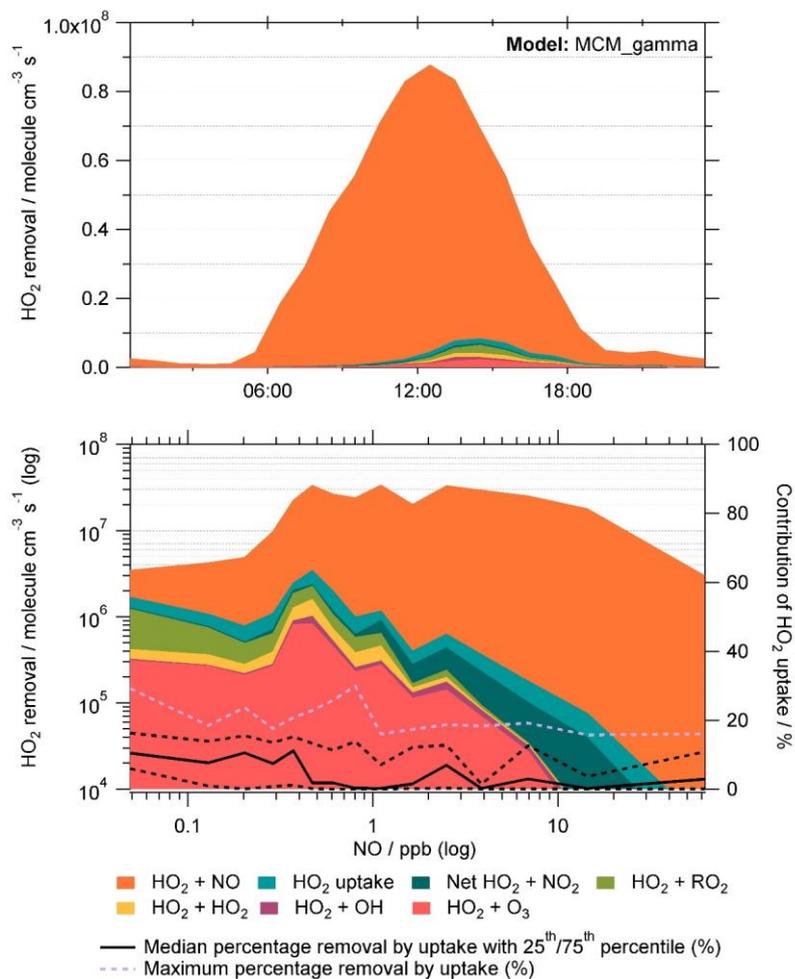


Figure 78. Rate of destruction analysis (RODA) showing the dominant loss pathways of HO₂ within MCM_gamma shown as (a) a diurnal variation and (b) as a function of NO mixing ratio (ppb). Median removal of HO₂ by uptake (%) as a function of NO (ppb) is shown as solid black line in (b), with 25th/75th percentile shown as the black dashed lines. Maximum percentage removal by uptake for a given NO mixing ratio is shown as a lilac dashed line.

558 As shown in the RODA, the dominant loss pathway of HO₂ is HO₂ + NO across the entire
 559 campaign (90 ± 14 % of total loss), followed by HO₂ + RO₂ (3.5 ± 8.1 % of total loss). This is
 560 expected due to high levels of NO_x in Beijing, especially during the day. As seen in the RODA
 561 diurnal, the HO₂ + NO loss pathway peaks at midday following the morning peak in NO mixing
 562 ratio due to rush hour traffic. As NO mixing ratio decreases, the relative importance of other

563 loss pathways of HO₂ increases. At the lowest NO mixing ratio, i.e. < 0.1 ppb NO, the loss
 564 pathways of HO₂ within MCM_gamma with the largest contribution to total loss were HO₂ +
 565 NO (55 ± 19 %), HO₂ + RO₂ (23 ± 17 %) and HO₂ + O₃ (9.3 ± 4.1 %). It is worth noting that
 566 as the NO mixing ratio decreases the relative importance of HO₂ removal by O₃ increases
 567 presumably due to the titration reaction of O₃ with NO decreasing (and hence higher observed
 568 [O₃]). This could be important when considering policy changes with NO_x pollution in China
 569 decreasing in recent years. The contribution of the various loss pathways of HO₂ to total HO₂
 570 loss within MCM_gamma under low (< 0.1 ppb) and high (>0.1 ppb) NO are compared in
 571 [Table 4](#).

	HO ₂ +O ₃	HO ₂ +OH	HO ₂ +HO ₂	HO ₂ +RO ₂	Net HO ₂ +NO ₂	HO ₂ +NO	uptake
Low NO (< 0.1 ppb)	9.3 ± 4.1	0.1 ± 0.1	3.0 ± 1.8	23 ± 17	2.4 ± 3.0	55 ± 19	7.3 ± 7.3
High NO (> 0.1 ppb)	1.8 ± 2.3	0.2 ± 0.3	0.8 ± 1.3	2.0 ± 4.4	0.4 ± 1.2	93 ± 9.0	1.9 ± <0.01

572 **Table 4.** Average relative percentage contribution of individual HO₂ loss pathways to the total loss of HO₂ within
 573 MCM_gamma, averaged for days when NO was low, (< 0.1 ppb) and high (> 0.1 ppb). Net HO₂+NO₂ refers to
 574 HO₂+NO₂→HO₂NO₂ minus HO₂NO₂→HO₂+NO₂.

575 Though there is not a strong dependence of HO₂ aerosol uptake loss pathway on NO mixing
 576 ratio for the calculated γ_{HO_2} (av. 0.07 ± 0.035) within MCM_gamma, it can be seen that at the
 577 lowest NO mixing ratios an average of ~7 % of total HO₂ loss is due to uptake, with a maximum
 578 at the lowest NO of ~29% (shown as lilac dashed line in [Figure 7](#)). This is a significant
 579 loss of HO₂, especially on days where the NO mixing ratio is low and the aerosol surface area
 580 is high, highlighting that the uptake of HO₂ onto aerosols could be important, and will be
 581 increasingly so at lower NO.

582 3.3.2 Comparison to γ_{HO_2} fixed at 0.2

583 While the maximum γ_{HO_2} calculated using the Song parameterisation for the summer AIRPRO
 584 campaign was 0.15, to provide context with previous modelling studies, the commonly used
 585 fixed value of $\gamma_{HO_2}=0.2$ was added into the MCM_base model to give the MCM_SA model.
 586 The average median diurnals of modelled OH, HO₂ and RO₂ (molecule cm⁻³) for MCM_base,
 587 MCM_gamma and MCM_SA are shown in [Figure 6](#).

588 In comparison to calculated γ_{HO_2} in MCM_gamma, a fixed $\gamma_{HO_2}=0.2$ had a more significant
 589 effect on radical concentrations. While the median diurnal shows that the RO₂ concentration
 590 was not significantly affected by the addition of HO₂ uptake, the over-prediction seen in the
 591 average median HO₂ concentration compared to the measurements at the 14:30 peak decreased

Formatted: Font: 12 pt, Not Bold

Formatted: Font: 12 pt, Not Bold, Not Italic

Formatted: Font: 12 pt, Not Bold

Formatted: Font: 12 pt, Not Bold

Formatted: Font: 12 pt, Not Bold, Not Italic

592 from a factor of ~2.9 in MCM_base to ~2.3. A plot of measured to modelled ratio of HO₂ as a
593 function of aerosol surface area is shown in Figure 4 of Supplementary Information for both
594 MCM_gamma and MCM_SA. OH radical concentrations were still relatively well reproduced
595 with early afternoon OH concentrations predicted better though this is due to a shift in the
596 modelled peak compared to the measured concentration peaking at midday. The ability of the
597 model to reproduce the NO dependence of radical concentrations with the addition of
598 As seen in Figure 9, the addition of $\gamma_{HO_2} = 0.2$ is discussed in Section 1.3 of Supplementary
599 Information.
600 ~~affected the ability of the model to reproduce the NO dependence of radical concentrations.~~
601 ~~While MCM_base over predicts HO₂ below 1 ppb NO, the over prediction of HO₂ decreases~~
602 ~~below 1 ppb NO for MCM_SA with HO₂ being well reproduced at the lowest NO mixing ratios~~
603 ~~(i.e. < 0.1 ppb) due to the relative increase in the importance of HO₂ uptake as a sink of HO₂.~~
604 ~~Modelled RO₂ is not significantly affected by the addition of HO₂ uptake at any NO mixing~~
605 ~~ratio. The modelled concentration of OH is under predicted for the entire range of NO mixing~~
606 ~~ratios compared to measured values, though only slightly between 1 and 6 ppb NO. Below~~
607 ~~4 ppb NO, the underprediction of OH by MCM_SA increases compared to MCM_base due~~
608 ~~most likely to loss of HO₂ onto aerosols competing with loss via NO to give OH. Budget~~
609 ~~analysis done by Whalley et al., 2021, showcases that with a reduction in over prediction of~~
610 ~~modelled HO₂, OH is under predicted revealing a missing OH source.~~

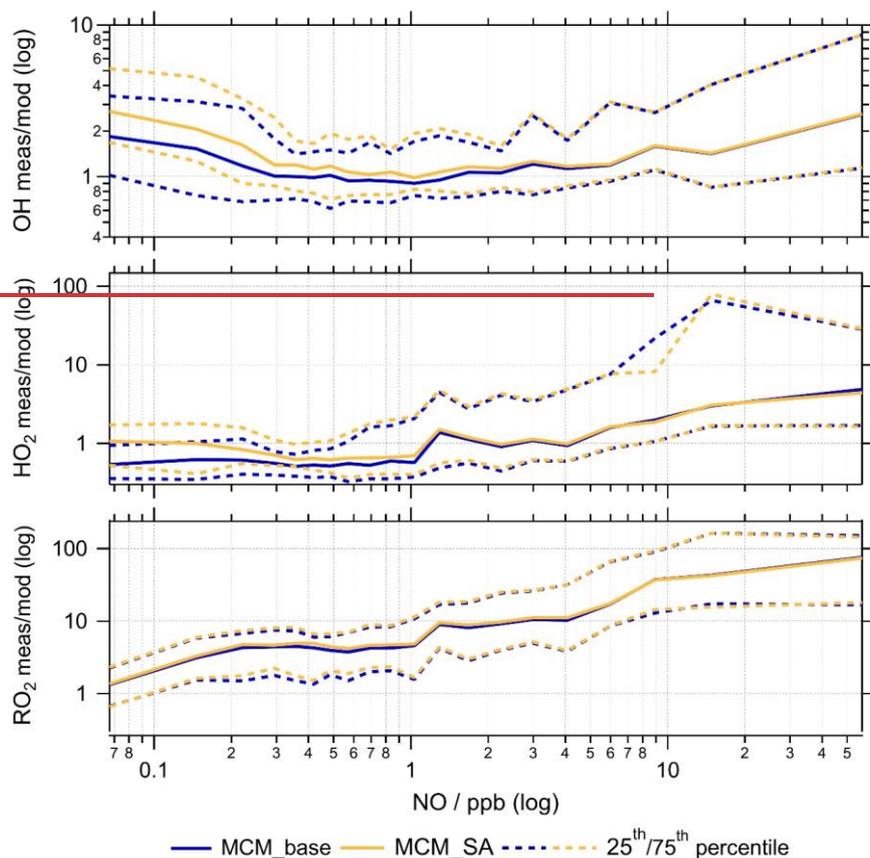


Figure 9. Ratio of measured to modelled OH, HO₂ and RO₂ radical concentrations using the MCM_base (blue) and MCM_SA (yellow) model binned over the range of NO mixing ratios (ppb) for the summer AIRPRO campaign. Solid lines show the median average measured to modelled radical concentration. Dashed lines show the 25th/75th percentile.

611 Analysis of the RODA for MCM_SA shows that with $\gamma_{HO_2} = 0.2$ HO₂ aerosol uptake is a
 612 significant contributor to total loss of HO₂ ($8.1 \pm 13 \%$, averaged for all NO mixing ratios).
 613 However, for all NO mixing ratios HO₂ + NO is still the dominant loss pathway ($86 \pm 18 \%$),
 614 as expected. At the lowest NO mixing ratios (i.e. < 0.1 ppb) an average of ~29 % of total HO₂
 615 loss is due to uptake, with a maximum at the lowest NO of ~78%, shown in [Figure 8](#) [Figure 10](#).
 616 The contribution of the various loss pathways of HO₂ to total HO₂ loss within MCM_gamma
 617 under low (< 0.1 ppb) and high (> 0.1 ppb) NO are compared in [Table 5](#) [Table 5](#). The comparison

Formatted: Font: 12 pt, Not Bold

Formatted: Font: 12 pt, Not Bold, Not Italic

Formatted: Font: 12 pt, Not Bold

Formatted: Font: 12 pt, Not Bold, Not Italic

618 of percentage contribution of HO₂ uptake to total HO₂ removal binned against NO mixing ratio
 619 (ppb) for MCM_gamma and MCM_SA RODA is shown in [Figure 8](#)~~Figure 10~~.

	HO ₂ +O ₃	HO ₂ +OH	HO ₂ +HO ₂	HO ₂ +RO ₂	Net HO ₂ +NO ₂	HO ₂ +NO	uptake
Low NO (< 0.1 ppb)	6.9 ± 3.5	0.1 ± 0.1	1.7 ± 1.4	17 ± 14	1.6 ± 2.2	44 ± 24	29 ± 24
High NO (> 0.1 ppb)	1.8 ± 2.1	0.2 ± 0.2	0.6 ± 1.0	1.7 ± 3.8	0.4 ± 1.0	89 ± 13	6.5 ± 9.7

620 **Table 5.** Average relative percentage contribution of individual HO₂ loss pathways to the total loss of HO₂ within
 621 MCM_SA (fixed $\gamma_{HO_2} = 0.2$), averaged for days when NO was low, (< 0.1 ppb) and high (> 0.1 ppb). Net
 622 HO₂+NO₂ refers to HO₂+NO₂→HO₂NO₂ minus HO₂NO₂→HO₂+NO₂.

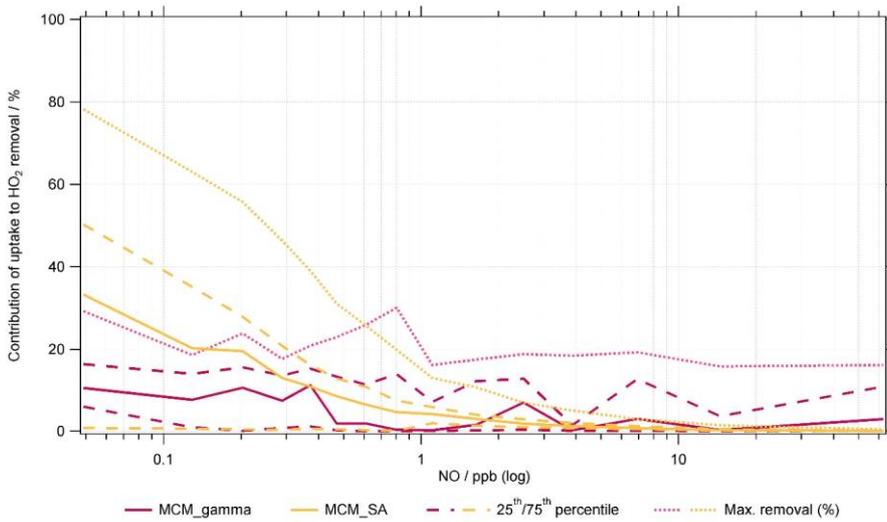


Figure 8~~10~~. Average percentage contribution of HO₂ uptake to total HO₂ removal within MCM_gamma (pink line, $\gamma_{HO_2} = 0.070 \pm 0.035$) and MCM_SA model (yellow line, $\gamma_{HO_2} = 0.2$) for Summer AIRPRO campaign plotted as a function of NO mixing ratio (ppb). Dashed lines represent the 25th/75th percentiles. Dotted lines represent maximum removal.

623 3.3.3 Effect of γ_{HO_2} on the O₃ regime

624 ~~3.3.3.11.1.1.1 Calculation of L_N/Q and absolute O₂ sensitivity~~

625 ~~First introduced by Kleinman et al., 1997, L_N/Q is the ratio of radical loss via NO_x to total~~
 626 ~~primary radical production and is used as a means of determining O₂ production sensitivity to~~
 627 ~~VOCs and NO_x (Kleinman, 2000; Kleinman et al., 1997; Kleinman et al., 2001). This method~~
 628 ~~was then built on by Sakamoto et al., 2019 who included loss of peroxy radicals~~
 629 ~~(XO₂ + HO₂ + RO₂) onto aerosol surfaces within the calculation of O₂ sensitivity.~~

Formatted: Font: 12 pt, Not Bold

Formatted: Font: 12 pt, Not Bold, Not Italic

630 ~~The only source of tropospheric O_3 is by the reaction of peroxy radicals with NO , while the~~
 631 ~~main source of XO_2 species is via the reaction of OH with VOCs.~~



632 ~~The O_3 production rate in the troposphere is therefore:~~

$$\cancel{P(O_3) = k_{HO_2+NO} [HO_2][NO] + k_{RO_2+NO} [RO_2][NO]} \quad (2)$$

633 ~~where k_{HO_2+NO} and k_{RO_2+NO} are the bimolecular rate constants for the reaction of HO_2 and~~
 634 ~~RO_2 with NO .~~

635 ~~The production rate of OH , HO_2 and RO_2 radicals, Q , must equal the loss rates:~~

$$\cancel{Q = L_p + L_{NO} + L_{RR}} \quad (3)$$

636 ~~where L_p is the loss rate of radicals onto aerosol particles, L_{NO} is the loss rate of radicals via~~
 637 ~~reaction with NO_x species and L_{RR} is the loss rate of radicals via radical-radical reactions to give~~
 638 ~~peroxides.~~

$$\cancel{L_p = k_{HO_2+uptake} [HO_2] + k_{RO_2+uptake} [RO_2] = k_p [YO_2]} \quad (4)$$

$$\cancel{L_{NO} \sim k_{NO_2+OH} [NO_2][OH]} \quad (5)$$

$$\cancel{L_{RR} = 2(k_{HO_2+HO_2} [HO_2]^2 + k_{RO_2+HO_2} [HO_2][RO_2])} \quad (6)$$

639 ~~where $k_{HO_2+uptake}$ is the rate constant for the loss of HO_2 onto aerosol surfaces, $k_{RO_2+uptake}$ is~~
 640 ~~the rate constant for the loss of RO_2 onto aerosol surfaces, k_{NO_2+OH} is the bimolecular rate~~
 641 ~~constant for the reaction of NO_2 with OH , $k_{HO_2+HO_2}$ is the bimolecular rate constant for the~~
 642 ~~self reaction of HO_2 and $k_{RO_2+HO_2}$ is the bimolecular rate constant for the reaction of RO_2 with~~
 643 ~~HO_2 .~~

644 ~~For radical loss onto aerosol surfaces, the rate constant is given as a function of the reactive~~
 645 ~~uptake coefficient, γ_{NO_2} , aerosol particle surface area ($cm^2 \cdot cm^{-3}$) and mean thermal velocity~~
 646 ~~($cm \cdot s^{-1}$), given by $v = \sqrt{2RT/\pi M}$ with R , T and M as the gas constant, the absolute temperature~~
 647 ~~and the molar mass of species respectively.~~

$$\cancel{k_{radical\ uptake} = \frac{\gamma_{NO_2} \times SA \times v}{4}} \quad (7)$$

648 ~~According to the method described in Sakamoto et al., 2019, the ratio of radical loss to NO_x to~~
 649 ~~primary O_3 production including radical loss via aerosol uptake, $\frac{L_{RR}}{Q}$ is defined as follows:~~

$$\frac{L_N}{Q} = \frac{1}{1 + \left(\frac{(2k_{HO_2} [XO_2] + k_{OH+VOC})k_{OH+VOC} [VOC]}{(1-\alpha)k_{HO_2+NO} [NO]k_{NO_2+OH} [NO_2]} \right)} \quad (8)$$

650 where k_{OH+VOC} is the bimolecular rate constant for the loss of OH via reaction with VOCs and
 651 $(1-\alpha)$ is the fraction of XO_2 that is HO_2 .

652 The relative sensitivity of O_3 production to NO_x and VOCs is described by:

$$\frac{\delta \ln P(O_3)}{\delta \ln [NO_x]} = (1-\chi) \left(\frac{1 - \frac{2L_N}{Q}}{1 - \frac{1L_N}{Q}} \right) + \chi \left(1 - \frac{2L_N}{Q} \right) \quad (9)$$

$$\frac{\delta \ln P(O_3)}{\delta \ln [VOC]} = (1-\chi) \left(\frac{\frac{1L_N}{Q}}{1 - \frac{1L_N}{Q}} \right) + \chi \frac{L_N}{Q} \quad (10)$$

653 where $\chi = \frac{L_N}{L_N + L_V}$. The O_3 regime transition point, where $\frac{\delta \ln P(O_3)}{\delta \ln [NO_x]} = \frac{\delta \ln P(O_3)}{\delta \ln [VOC]}$, is given by $\frac{L_N}{Q_{trans}}$

$$\frac{L_N}{Q_{trans}} = \frac{1}{2} (1-\chi) + \frac{1}{3}\chi \quad (11)$$

654 Absolute O_3 sensitivity was introduced by Sakamoto et al., 2019, and allows for the assessment
 655 of how reduction in O_3 precursors could contribute to reduction in $P(O_3)$ by integrating over
 656 time and area. The absolute sensitivity of O_3 production to VOC and NO_x is then described by:

$$Absolute P(O_3) = \frac{\delta P(O_3)}{\delta \ln [X]} = P(O_3) \frac{\delta P(O_3)}{\delta \ln [X]} \quad (12)$$

657 where X is NO_x or VOC.

658 $\frac{L_N}{Q}$ was calculated for all model runs, MCM_base, MCM_gamma and MCM_SA using
 659 modelled $[HO_2]$ and $[RO_2]$ concentrations but measured values of $[NO]$ and $[NO_2]$, to
 660 investigate the effect on the O_3 regime of adding HO_2 aerosol uptake into the model. The time
 661 series of calculated $\frac{L_N}{Q}$ for all models, in addition to the regime transition point, $\frac{L_N}{Q_{trans}}$ for the
 662 entire campaign is shown in [Figure 9](#) ~~Figure 11~~.

663 When $\frac{L_N}{Q} < \frac{L_N}{Q_{trans}}$, this is defined as a NO_x -sensitive regime, meaning that small changes in NO_x
 664 will affect the rate of in situ O_3 production. This can be seen on a few days across the campaign,
 665 specifically in the afternoon, due to NO_x peaking in the morning due to traffic emissions before
 666 rapidly decreasing in the afternoon which pushes the O_3 regime on certain days from VOC-

Formatted: Font: 12 pt, Not Bold

667 limited to NO_x-limited. However, for the majority of the campaign, the O₃ production regime
 668 is VOC-limited, for all models, meaning that O₃ production rates will not be significantly
 669 affected by small changes in NO_x.

670 Binning $\frac{L_N}{Q}$ against NO mixing ratio (ppb), in ~~Figure 10~~ **Figure 12**, shows the change from VOC
 671 to NO_x-limited regime at very low NO mixing ratios for MCM_base, MCM_gamma and
 672 MCM_SA. As aerosol uptake is added the transition to NO_x-limited regime occurs at higher
 673 NO, with average median transition point occurring at ~ 0.2 ppb NO for MCM_gamma
 674 (average $\gamma_{HO_2} = 0.070 \pm 0.035$) and at ~0.5 ppb NO for MCM_SA (fixed $\gamma_{HO_2} = 0.2$). This
 675 suggests that a reduction in PM (and therefore uptake of HO₂ onto aerosols) would delay the
 676 transition to a NO_x-sensitive regime until lower NO_x levels are reached. Therefore, any
 677 emissions policy aimed at reduced NO_x to decrease O₃ levels would not be as effective if PM
 678 is decreasing at the same time.

Formatted: Font: 12 pt, Not Bold
 Formatted: Font: 12 pt, Not Bold, Not Italic

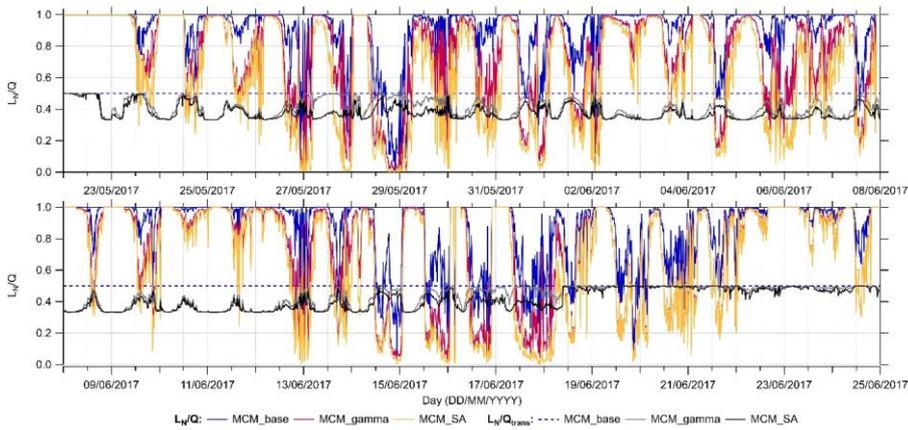


Figure 9H. Time series of calculated $\frac{L_N}{Q}$ and $\frac{L_N}{Q_{trans}}$ values for MCM_base (blue), MCM_gamma (pink) and MCM_SA (yellow) models across the entire summer AIRPRO campaign. $\frac{L_N}{Q_{trans}}$ for MCM_gamma is shown as grey line, while $\frac{L_N}{Q_{trans}}$ for MCM_SA is the black line.

679

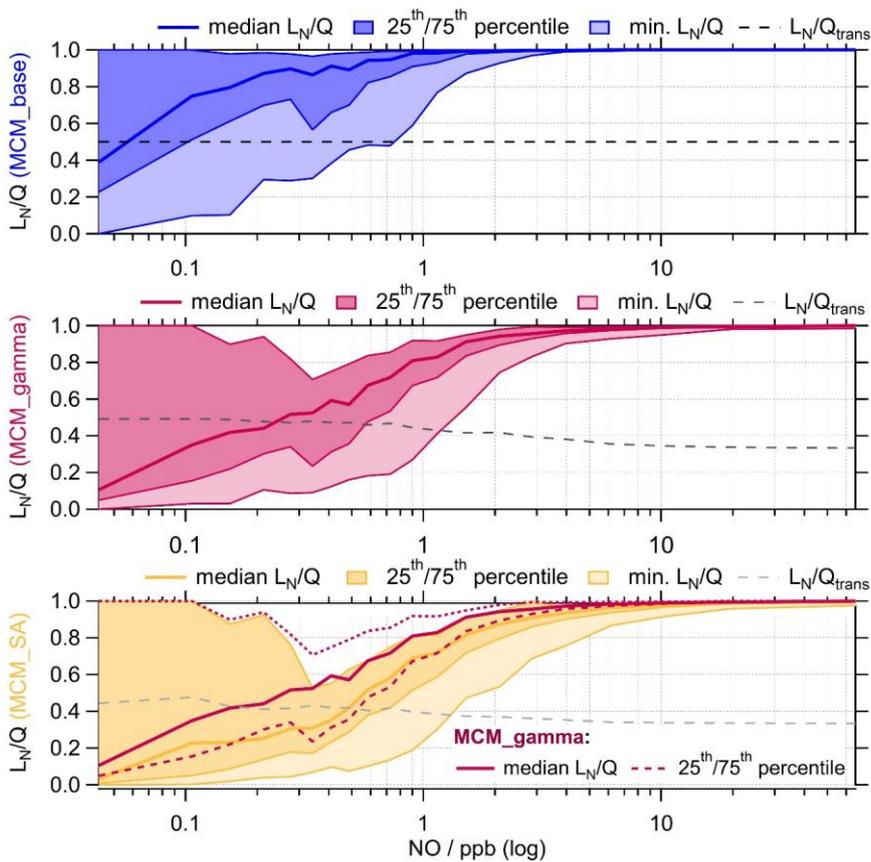


Figure 1012. $\frac{L_N}{Q}$ for MCM_base (blue, top panel), MCM_gamma (pink, middle panel) and MCM_SA (yellow, bottom panel) binned against the log of measured NO mixing ratio for the entire summer AIRPRO campaign. $\frac{L_N}{Q_{trans}}$ for MCM_base (black dashed line) taken as 0.5 for entire range of NO mixing ratios. $\frac{L_N}{Q_{trans}}$ for MCM_gamma (dark grey dashed line) and MCM_SA (light grey dashed line) calculated using equation 140. 25th/75th percentiles and minimum $\frac{L_N}{Q}$ are plotted to show full spread of data for each model scenario.

680 The average median diurnal of absolute $P(O_3)$, $\frac{\delta P(O_3)}{\delta \ln [X]}$, for the MCM_gamma and MCM_SA
 681 over the entire campaign is shown in [Figure 11](#)[Figure 13](#). The time series of absolute $P(O_3)$,
 682 averaged up to a daily time resolution, across the entire measurement period can be found in
 683 Supplementary Information as SI [Figure 52](#).

Formatted: Font: 12 pt, Not Bold

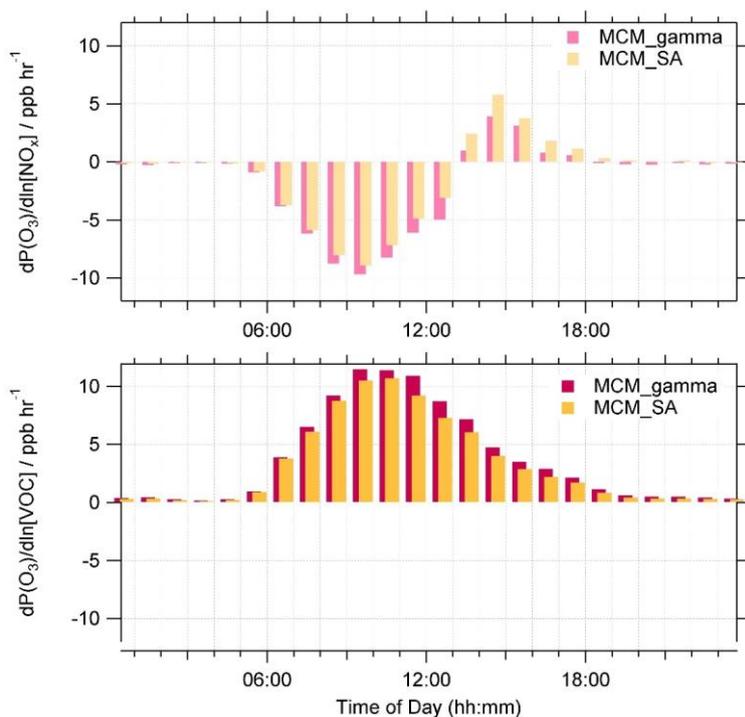


Figure 1113. Average median diurnal of absolute O₃ sensitivity to NO_x (top panel) and VOC (bottom panel) in ppbV h⁻¹ for MCM_gamma (pink) and MCM_SA (yellow) across the entire summer AIRPRO campaign. MCM_gamma includes γ_{HO_2} calculated using the Song parameterisation (av. 0.070 ± 0.035) while MCM_SA includes γ_{HO_2} at a fixed value of 0.2. All diurnals are 60 minute averages.

684 As expected from $\frac{LN}{Q}$ calculations, calculations of absolute O₃ production sensitivity showcase
 685 that for both MCM_gamma and MCM_SA, on average, the O₃ regime was VOC sensitive
 686 throughout the day with NO_x sensitivity increasing in the afternoons. On a few days, when low
 687 NO mixing ratio coincided with high SA, the O₃ regime can be seen shifting from VOC to NO_x
 688 limited. An example of this can be found in SI Figure 63, for the 17/06/2017 and 18/06/2017
 689 when the average NO mixing ratio was 0.41 ± 0.50 ppb and the average SA was $(8.4 \pm 6.2) \times$
 690 10^{-6} cm² cm⁻³. With an increase in γ_{HO_2} between MCM_gamma and MCM_SA, the sensitivity
 691 of O₃ regime to VOC decreased but sensitivity to NO_x increased. This effect could be important
 692 for areas where O₃ production regime is NO_x sensitive or less strongly VOC sensitive. With
 693 NO_x levels reportedly decreasing across China in recent years (Krotkov et al., 2016; Liu et al.,
 694 2016; Miyazaki et al., 2017; Van Der A et al., 2017), O₃ production regimes would be expected
 695 to move more towards NO_x-sensitive regimes in urban China. However, with concomitant

696 reduction in PM (Ma et al., 2016b; Lin et al., 2018), this transition to a NO_x-sensitive regime
697 may be delayed until lower NO_x levels are reached.

698 Our result for the Beijing campaign are consistent with the results of Song et al., 2022 which
699 concluded that for the conditions of the Wangdu campaign the addition of HO₂ uptake does not
700 change the overall O₃ sensitivity regime throughout the campaign. However, the shift in O₃
701 sensitivity regime from VOC-limited to NO_x-limited from the consideration of HO₂ uptake
702 could be important for areas with lower NO_x and high aerosol particle loading.

703 **4 Conclusions**

704 Using the Song parameterisation, the heterogeneous uptake coefficient of HO₂, γ_{HO_2} , was
705 calculated for the summer AIRPRO campaign in Beijing, 2017 as a function of measured
706 [Cu²⁺]_{eff}, [ALWC] and [PM]. The calculated average $\gamma_{HO_2} = 0.070 \pm 0.035$ (ranging from 0.002
707 to 0.15 across the campaign) was significantly lower than the fixed value of $\gamma_{HO_2} = 0.2$
708 commonly used in modelling studies. This calculated value was similar, however, to values
709 calculated for the Wangdu 2014 summer campaign in China (Tan et al., 2020; Song et al.,
710 2020). Using the calculated γ_{HO_2} , the OH, HO₂ and RO₂ radical concentrations were modelled
711 using the Master Chemical Mechanism, and compared to the measured campaign values, with
712 and without the addition of HO₂ aerosol uptake. Due to the low calculated value of γ_{HO_2} , and
713 the high levels of NO, rate of destruction analysis showed the dominant HO₂ loss pathway to
714 be HO₂ + NO for all NO mixing ratios with HO₂ uptake not contributing significantly to the
715 loss of HO₂ (< 2 %). However, at the lowest NO mixing ratios (i.e. < 0.1 ppb) HO₂ loss onto
716 aerosols contributed up to a maximum of 29 % of the total HO₂ loss. Using the modelled HO₂
717 and RO₂ radical concentrations for model scenarios with and without HO₂ uptake, showed that
718 on average the O₃ production regime was VOC-limited across the entire campaign with the
719 exception of several days with low NO mixing ratio where the regime tended towards NO_x-
720 limited, meaning that small changes in NO_x would not have a large effect on the O₃ production
721 for this summer period in Beijing, however changes in HO₂ uptake could. While the addition
722 of the calculated uptake coefficient did not change the overall O₃ regime across the campaign,
723 with the O₃ production regime remaining strongly VOC-limited, the transition from a VOC-
724 sensitive to NO_x-sensitive O₃ regime occurs at higher NO_x. This means that for Beijing, where
725 the O₃ production regime is strongly VOC-sensitive and NO_x levels are high, any policy
726 looking to reduce O₃ via the reduction of NO_x needs to consider concurrent PM reduction
727 policies which may affect HO₂ uptake. In cleaner environments, where NO_x levels are lower,

728 but aerosol surface area is still high, lower values of γ_{HO_2} , i.e. less than 0.2, could have a more
729 significant effect on both overall HO₂ concentration and the O₃ production regime.

730 *Data availability.* Data presented in this study can be obtained from authors upon request
731 (d.e.heard@leeds.ac.uk)

732 *Author contributions.* LKW, EJS, RWM, CY and DEH carried out the radical measurements.
733 LKW and EJS developed the model and JED performed the calculations. JDL, FS, JRH, RED,
734 MS, JFH, ACL, AM, SDW, AB, TJB, HC, BO, CJP, CNH, RLJ, LRC, LJK, WJFA, WJB, SS,
735 JX, TV, ZS, RMH, SK, SG, YS, WX, SY, LW, PF and XW provided logistical support and
736 supporting data to constrain the model. JED prepared the manuscript with contributions from
737 all co-authors.

738 *Competing interests.* The authors declare that they have no conflict of interest.

739 *Acknowledgements.* We are grateful to the Natural Environmental Research Council for
740 funding a SPHERES PhD studentship (Joanna E. Dyson). We are grateful to Tuan Vu for
741 providing supervision and supporting data.

742 **5 References**

743 Bohn, B., Heard, D. E., Mihalopoulos, N., Plass-Dülmer, C., Schmitt, R., and Whalley, L. K.:
744 Characterisation and improvement of j(O¹D) filter radiometers, *Atmos. Meas. Tech.*, 9, 3455-
745 3466, <https://doi.org/10.5194/amt-9-3455-2016>, 2016.

746 Brauer, M., Freedman, G., Frostad, J., van Donkelaar, A., Martin, R. V., Dentener, F.,
747 Dingenen, R. v., Estep, K., Amini, H., Apte, J. S., Balakrishnan, K., Barregard, L., Broday,
748 D., Feigin, V., Ghosh, S., Hopke, P. K., Knibbs, L. D., Kokubo, Y., Liu, Y., Ma, S.,
749 Morawska, L., Sangrador, J. L. T., Shaddick, G., Anderson, H. R., Vos, T., Forouzanfar, M.
750 H., Burnett, R. T., and Cohen, A.: Ambient Air Pollution Exposure Estimation for the Global
751 Burden of Disease 2013, *Environ. Sci. Technol.*, 50, 79-88,
752 <https://doi.org/10.1021/acs.est.5b03709>, 2016.

753 Commane, R., Floquet, C. F. A., Ingham, T., Stone, D., Evan, M. J., and Heard, D. E.:
754 Observations of OH and HO₂ radicals over West Africa, *Atmos. Chem. Phys.*, 10, 8783-8801,
755 <https://doi.org/10.5194/acp-10-8783-2010>, 2010.

756 Cooper, P. L. and Abbatt, J. P. D.: Heterogeneous Interactions of OH and HO₂ Radicals with
757 Surfaces Characteristic of Atmospheric Particulate Matter, *The Journal of Physical*
758 *Chemistry*, 100, 2249-2254, <https://doi.org/10.1021/jp952142z>, 1996.

759 Crilley, L. R., Kramer, L., Pope, F. D., Whalley, L. K., Cryer, D. R., Heard, D. E., Lee, J. D.,
760 Reed, C., and Bloss, W. J.: On the interpretation of in situ HONO observations via
761 photochemical steady state, *Faraday Discuss.*, 189, 191-212,
762 <https://doi.org/10.1039/c5fd00224a>, 2016.

763 Dunmore, R., Hopkins, J., Lidster, R., Lee, J., Evans, M., Rickard, A., Lewis, A., and
764 Hamilton, J.: Diesel-related hydrocarbons can dominate gas phase reactive carbon in
765 megacities, *Atmos. Chem. Phys.*, 15, 9983-9996, <https://doi.org/10.5194/acp-15-9983-2015>,
766 2015.

767 Forster, P., Ramaswamy, V., Artaxo, P., Berntsen, T., Betts, R., Fahey, D. W., Haywood, J.,
768 Lean, J., Lowe, D. C., Myhre, G., Nganga, J., Prinn, R., Raga, G., Schulz, M., and Dorland,
769 R. V.: Chapter 2. Changes in atmospheric constituents and in radiative forcing. , *Climate*
770 *Change 2007. The Physical Science Basis*, 2007.

771 Fountoukis, C. and Nenes, A.: ISORROPIA II: a computationally efficient thermodynamic
772 equilibrium model for K^+ - Ca^{2+} - Mg^{2+} - NH_4^+ - Na^+ - SO_4^{2-} - NO_3^- - Cl^- - H_2O aerosols, *Atmos. Chem.*
773 *Phys.*, 7, 4639-4659, <https://doi.org/10.5194/acp-7-4639-2007>, 2007.

774 Fuchs, H., Holland, F., and Hofzumahaus, A.: Measurement of tropospheric RO_2 and HO_2
775 radicals by a laser-induced fluorescence instrument, *The Review of scientific instruments*, 79,
776 084104, <https://doi.org/10.1063/1.2968712>, 2008.

777 Gakidou, E., Afshin, A., Abajobir, A. A., Abate, K. H., Abbafati, C., Abbas, K. M., Abd-
778 Allah, F., Abdulle, A. M., Abera, S. F., and Aboyans, V.: Global, regional, and national
779 comparative risk assessment of 84 behavioural, environmental and occupational, and
780 metabolic risks or clusters of risks, 1990–2016: a systematic analysis for the Global Burden
781 of Disease Study 2016, *The Lancet*, 390, 1345-1422, [https://doi.org/10.1016/S0140-](https://doi.org/10.1016/S0140-6736(18)32279-7)
782 [6736\(18\)32279-7](https://doi.org/10.1016/S0140-6736(18)32279-7), 2017.

783 George, I. J., Matthews, P. S. J., Whalley, L. K., Brooks, B., Goddard, A., Baeza-Romero,
784 M., and Heard, D. E.: Measurements of uptake coefficients for heterogeneous loss of HO_2
785 onto submicron inorganic salt aerosols., *Phys. Chem. Chem. Phys.*, 15, 12829-12845,
786 <https://doi.org/10.1039/c3cp51831k>, 2013.

787 Hopkins, J. R., Jones, C. E., and Lewis, A. C.: A dual channel gas chromatograph for
788 atmospheric analysis of volatile organic compounds including oxygenated and monoterpene
789 compounds., *J. Environ. Monit.*, 13, 2268-2276, <https://doi.org/10.1039/C1EM10050E>, 2011.

790 Ivatt, P. D., Evans, M. J., and Lewis, A. C.: Suppression of surface ozone by an aerosol-
791 inhibited photochemical ozone regime, *Nat. Geosci.*, 15, 536-540,
792 <https://doi.org/10.1038/s41561-022-00972-9>, 2022.

793 Jacob, D. J.: Heterogeneous chemistry and tropospheric ozone, *Atmos. Environ.*, 34, 2131-
794 2159, [https://doi.org/10.1016/S1352-2310\(99\)00462-8](https://doi.org/10.1016/S1352-2310(99)00462-8), 2000.

795 Jin, Y., Andersson, H., and Zhang, S.: Air Pollution Control Policies in China: A
796 Retrospective and Prospects, *Int. J. Environ. Res. Public Health*, 13,
797 <https://doi.org/10.3390/ijerph13121219>, 2016.

798 Kanaya, Y. G., Cao, R. Q., Kato, S. G., Miyakawa, Y. K., Kajii, Y., Tanimoto, H., Yokouchi,
799 Y., Mochida, M., Kawamura, K., and Akimoto, H.: Chemistry of OH and HO₂ radicals
800 observed at Rishiri Island, Japan, in September 2003: Missing daytime sink of HO₂ and
801 positive nighttime correlations with monoterpenes, *J. Geophys. Res. Atmos.*, 112, D11308,
802 <https://doi.org/10.1029/2006JD007987>, 2007.

803 Kleinman, L. I.: Ozone process insights from field experiments – part II: Observation-based
804 analysis for ozone production, *Atmos. Environ.*, 34, 2023-2033,
805 [https://doi.org/10.1016/S1352-2310\(99\)00457-4](https://doi.org/10.1016/S1352-2310(99)00457-4), 2000.

806 Kleinman, L. I., Daum, P. H., Lee, Y.-N., Nunnermacker, L. J., Springston, S. R., Weinstein-
807 Lloyd, J., and Rudolph, J.: Sensitivity of ozone production rate to ozone precursors, *Geophys.*
808 *Res. Lett.*, 28, 2903-2906, <https://doi.org/10.1029/2000GL012597>, 2001.

809 Kleinman, L. I., Daum, P. H., Lee, J. H., Lee, Y.-N., Nunnermacker, L. J., Springston, S. R.,
810 Newman, L., Weinstein-Lloyd, J., and Sillman, S.: Dependence of ozone production on NO
811 and hydrocarbons in the troposphere, *Geophys. Res. Lett.*, 24, 2299-2302,
812 <https://doi.org/10.1029/97GL02279>, 1997.

813 Krotkov, N. A., McLinden, C. A., Li, C., Lamsal, L. N., Celarier, E. A., Marchenko, S. V.,
814 Swartz, W. H., Bucsela, E. J., Joiner, J., Duncan, B. N., Boersma, K. F., Veefkind, J. P.,
815 Levelt, P. F., Fioletov, V. E., Dickerson, R. R., He, H., Lu, Z., and Streets, D. G.: Aura OMI
816 observations of regional SO₂ and NO₂ pollution changes from 2005 to 2015, *Atmos. Chem.*
817 *Phys.*, 16, 4605-4629, <https://doi.org/10.5194/acp-16-4605-2016>, 2016.

818 Lakey, P. S. J., George, I. J., Baeza-Romero, M., Whalley, L. K., and Heard, D. E.: Organics
819 substantially reduce HO₂ uptake onto aerosols containing transition metal ions. , *J. Phys.*
820 *Chem. A*, 120, 1421-1430, <https://doi.org/10.1021/acs.jpca.5b06316>, 2016.

821 Lakey, P. S. J., George, I. J., Whalley, L. K., Baeza-Romero, M., and Heard, D. E.:
822 Measurements of HO₂ uptake coefficients onto single component organic aerosols.,
823 *Environmental Science Technology*, 49, 4878-4885, <https://doi.org/10.1021/acs.est.5b00948>,
824 2015.

825 Le Breton, M., Bacak, A., Muller, J. B. A., Bannan, T. J., Kennedy, O., Ouyang, B., Xiao, P.,
826 Bauguitte, S. J. B., Shallcross, D. E., Jones, R. L., Daniels, M. J. S., Ball, S. M., and Percival,

827 C. J.: The first airborne comparison of N₂O₅ measurements over the UK using a CIMS and
828 BBCEAS during the RONOCO campaign, *Analytical Methods*, 6, 9731-9743,
829 <https://doi.org/10.1039/C4AY02273D>, 2014.

830 Levy, H.: Normal atmosphere: large radical and formaldehyde concentrations predicted,
831 *Science*, 173, 141-143, <https://doi.org/10.1126/science.173.3992.141>, 1971.

832 Li, H., Wang, D., Cui, L., Gao, Y., Huo, J., Wang, X., Zhang, Z., Tan, Y., Huang, Y., and
833 Cao, J. J. S. o. t. t. e.: Characteristics of atmospheric PM_{2.5} composition during the
834 implementation of stringent pollution control measures in shanghai for the 2016 G20 summit,
835 648, 1121-1129, <https://doi.org/10.1016/j.scitotenv.2018.08.219>, 2019.

836 Li, K., Jacob, D. J., Liao, H., Shen, L., Zhang, Q., and Bates, K.: Anthropogenic drivers of
837 2013-2017 trends in summer surface ozone in China, *Proceedings of the National Academy*
838 *of Sciences*, 116, 422-427, <https://doi.org/10.1073/pnas.1812168116>, 2018.

839 Lin, C. Q., Liu, G., Lau, A. K. H., Li, Y., Li, C. C., Fung, J. C. H., and Lao, X. Q.: High-
840 resolution satellite remote sensing of provincial PM_{2.5} trends in China from 2001 to 2015,
841 *Atmos. Environ.*, 180, 110-116, <https://doi.org/10.1016/j.atmosenv.2018.02.045>, 2018.

842 Liu, F., Zhang, Q., van der A, R. J., Zheng, B., Tong, D., Yan, L., Zheng, Y., and He, K.:
843 Recent reduction in NO_x emissions over China: synthesis of satellite observations and
844 emission inventories, *Environ. Res. Lett*, 11, 114002, [https://doi.org/10.1088/1748-](https://doi.org/10.1088/1748-9326/11/11/114002)
845 [9326/11/11/114002](https://doi.org/10.1088/1748-9326/11/11/114002), 2016.

846 Liu, Y.-H., Liao, W.-Y., Lin, X.-F., Li, L., and Zeng, X.-l.: Assessment of Co-benefits of
847 vehicle emission reduction measures for 2015–2020 in the Pearl River Delta region, China,
848 *Environ. Pollut.*, 223, 62-72, <https://doi.org/10.1016/j.envpol.2016.12.031>, 2017.

849 Ma, Z., Xu, J., Quan, W., Zhang, Z., Lin, W., and Xu, X.: Significant increase of surface
850 ozone at a rural site, north of eastern China, *Atmos. Chem. Phys.*, 16, 3969-3977,
851 [https://doi.org/10.5194/acp-](https://doi.org/10.5194/acp-16-3969-2016)
852 [16-3969-2016](https://doi.org/10.5194/acp-16-3969-2016), 2016a.

853 Ma, Z., Hu, X., Sayer, A. M., Levy, R., Zhang, Q., Xue, Y., Tong, S., Bi, J., Huang, L., and
854 Liu, Y.: Satellite-Based Spatiotemporal Trends in PM_{2.5} Concentrations: China, 2004-2013,
855 *Environ. Health Perspect.*, 124, 184-192, <https://doi.org/10.1289/ehp.1409481>, 2016b.

856 Mao, J., Fan, S., Jacob, D. J., and Travis, K. R.: Radical loss in the atmosphere from Cu-Fe
857 redox coupling in aerosols, *Atmos. Chem. Phys.*, 13, 509-519, [https://doi.org/10.5194/acp-](https://doi.org/10.5194/acp-13-509-2013)
858 [13-509-2013](https://doi.org/10.5194/acp-13-509-2013), 2013.

859 Mao, J., Jacob, D. J., Evans, M. J., Olson, J. R., Ren, X., Brune, W. H., Chair, J. M. S.,
860 Crounse, J. D., Spencer, K. M., Beaver, M. R., Wennberg, P. O., Cubison, M. J., Jimenez, J.
L., Fried, A., Weibring, P., Walega, J. G., Hall, S. R., Weinheimer, A. J., Cohen, R. C., Chen,

861 G., Crawford, J. H., McHaughton, C., Clarke, A. D., Jaegle, L., Fisher, J. K., Yantosca, R.
862 M., LeSager, P., and Carouge, C.: Chemistry of hydrogen oxide radicals (HO_x) in the arctic
863 troposphere in spring, *Atmos. Chem. Phys.*, 10, 5823-5838, [https://doi.org/10.5194/acp-10-](https://doi.org/10.5194/acp-10-5823-2010)
864 [5823-2010](https://doi.org/10.5194/acp-10-5823-2010), 2010.

865 Martinez, M., Harder, H., Kovacs, T. A., Simpas, J. B., Bassis, J., Leshner, R., Brune, W. H.,
866 Frost, G. J., Williams, E. J., Stroud, C. A., Jobson, B. T., Roberts, J. M., Hall, S. R., Shetter,
867 R. E., Wert, B., Fried, A., Alicke, B., Stutz, J., Young, V. L., White, A. B., and Zamora, R. J.:
868 OH and HO₂ concentrations, sources, and loss rates during the Southern Oxidants Study in
869 Nashville, Tennessee, summer 1999, *Journal of Geophysical Research: Atmospheres*, 108,
870 <https://doi.org/10.1029/2003JD003551>, 2003.

871 Matthews, P. S. J., Baeza-Romero, M., Whalley, L. K., and Heard, D. E.: Uptake of HO₂
872 radicals onto Arizona test dust particles using an aerosol flow tube, *Atmos. Chem. Phys.*, 14,
873 7397-7408, <https://doi.org/10.5194/acp-14-7397-2014>, 2014.

874 Miyazaki, K., Eskes, H., Sudo, K., Boersma, K. F., Bowman, K., and Kanaya, Y.: Decadal
875 changes in global surface NO_x emissions from multi-constituent satellite data assimilation,
876 *Atmos. Chem. Phys.*, 17, 807-837, <https://doi.org/10.5194/acp-17-807-2017>, 2017.

877 Mozurkewich, M., McMurry, P. H., Gupta, A., and Calvert, J. G.: Mass accommodation
878 coefficient for HO₂ radicals on aqueous particles, *J. Geophys. Res.*, 92, 4163-4170,
879 <https://doi.org/10.1029/JD092iD04p04163>, 1987.

880 Sakamoto, Y., Sadanaga, Y., Li, J., Matsuoka, K., Takemura, M., Fujii, T., Nakagawa, M.,
881 Kohno, N., Nakashima, Y., Sato, K., Nakayama, T., Kato, S., Takami, A., Yoshino, A.,
882 Murano, K., and Kajii, Y.: Relative and Absolute Sensitivity Analysis on Ozone Production
883 in Tsukuba, a City in Japan, *Environ. Sci. Technol.*, 53, 13629-13635,
884 <https://doi.org/10.1021/acs.est.9b03542>, 2019.

885 Shi, Z., Vu, T., Kotthaus, S., Harrison, R. M., Grimmond, S., Yue, S., Zhu, T., Lee, J., Han,
886 Y., Demuzere, M., Dunmore, R. E., Ren, L., Liu, D., Wang, Y., Wild, O., Allan, J., Acton,
887 W. J., Barlow, J., Barratt, B., Beddows, D., Bloss, W. J., Calzolari, G., Carruthers, D.,
888 Carslaw, D. C., Chan, Q., Chatzidiakou, L., Chen, Y., Crilley, L., Coe, H., Dai, T., Doherty,
889 R., Duan, F., Fu, P., Ge, B., Ge, M., Guan, D., Hamilton, J. F., He, K., Heal, M., Heard, D.,
890 Hewitt, C. N., Hollaway, M., Hu, M., Ji, D., Jiang, X., Jones, R., Kalberer, M., Kelly, F. J.,
891 Kramer, L., Langford, B., Lin, C., Lewis, A. C., Li, J., Li, W., Liu, H., Liu, J., Loh, M., Lu,
892 K., Lucarelli, F., Mann, G., McFiggans, G., Miller, M. R., Mills, G., Monk, P., Nemitz, E.,
893 O'Connor, F., Ouyang, B., Palmer, P. I., Percival, C., Popoola, O., Reeves, C., Rickard, A. R.,
894 Shao, L., Shi, G., Spracklen, D., Stevenson, D., Sun, Y., Sun, Z., Tao, S., Tong, S., Wang, Q.,

895 Wang, W., Wang, X., Wang, X., Wang, Z., Wei, L., Whalley, L., Wu, X., Wu, Z., Xie, P.,
896 Yang, F., Zhang, Q., Zhang, Y., Zhang, Y., and Zheng, M.: Introduction to the special issue
897 “In-depth study of air pollution sources and processes within Beijing and its surrounding
898 region (APHH-Beijing)”, *Atmos. Chem. Phys.*, 19, 7519-7546, [https://doi.org/10.5194/acp-](https://doi.org/10.5194/acp-19-7519-2019)
899 [19-7519-2019](https://doi.org/10.5194/acp-19-7519-2019), 2019.

900 Silver, B., Reddington, C. L., Arnold, S. R., and Spracklen, D. V.: Substantial changes in air
901 pollution across China during 2015–2017, *Environ. Res. Lett.*, 13, 114012,
902 <https://doi.org/10.1088/1748-9326/aae718>, 2018.

903 Slater, E. J.: Understanding radical chemistry in Beijing through observations and modelling,
904 School of Chemistry, University of Leeds, 2020.

905 Slater, E. J., Whalley, L. K., Woodward-Massey, R., Ye, C., Lee, J. D., Squires, F., Hopkins,
906 J. R., Dunmore, R. E., Shaw, M., Hamilton, J. F., Lewis, A. C., Crilley, L. R., Kramer, L.,
907 Bloss, W., Vu, T., Sun, Y., Xu, W., Yue, S., Ren, L., Acton, W. J. F., Hewitt, C. N., Wang,
908 X., Fu, P., and Heard, D. E.: Elevated levels of OH observed in haze events during
909 wintertime in central Beijing, *Atmos. Chem. Phys. Discuss.*, 2020, 1-43,
910 <https://doi.org/10.5194/acp-2020-362>, 2020.

911 Smith, K. R., Edwards, P. M., Evans, M. J., Lee, J. D., Shaw, M. D., Squires, F., Wilde, S.,
912 and Lewis, A. C.: Clustering approaches to improve the performance of low cost air pollution
913 sensors, *Faraday Discuss.*, 200, 621-637, <https://doi.org/10.1039/C7FD00020K>, 2017.

914 Sommariva, R., Haggerstone, A. L., Carpenter, L. J., Carslaw, N., Creasey, D. J., Heard, D.
915 E., Lee, J. D., Lewsi, A. C., Pilling, M. J., and Zador, J.: OH and HO₂ chemistry in clean
916 marine air during SOAPEX-2, *Atmos. Chem. Phys.*, 4, 839-856, [https://doi.org/10.5194/acp-](https://doi.org/10.5194/acp-4-839-2004)
917 [4-839-2004](https://doi.org/10.5194/acp-4-839-2004), 2004.

918 Song, H., Lu, K., Dong, H., Tan, Z., Chen, S., Zeng, L., and Zhang, Y.: Reduced Aerosol
919 Uptake of Hydroperoxyl Radical May Increase the Sensitivity of Ozone Production to
920 Volatile Organic Compounds, *Environ. Sci. Tech. Letts.*, 9, 22-29,
921 <https://doi.org/10.1021/acs.estlett.1c00893>, 2022.

922 Song, H., Chen, X., Lu, K., Zou, Q., Tan, Z., Fuchs, H., Wiedensohler, A., Moon, D. R.,
923 Heard, D. E., Baeza-Romero, M. T., Zheng, M., Wahner, A., Kiendler-Scharr, A., and Zhang,
924 Y.: Influence of aerosol copper on HO₂ uptake: a novel parameterized equation, *Atmos.*
925 *Chem. Phys.*, 20, 15835-15850, <https://doi.org/10.5194/acp-20-15835-2020>, 2020.

926 Stone, D., Whalley, L. K., Ingham, T., Edwards, P. M., Cryer, D. R., Brumby, C. A., Seakins,
927 P. W., and Heard, D. E.: Measurement of OH reactivity by laser flash photolysis coupled

928 with laser-induced fluorescence spectroscopy, *Atmos. Meas. Tech.*, 9, 2827-2844,
929 <https://doi.org/10.5194/amt-9-2827-2016>, 2016.

930 Taketani, F., Kanaya, Y., and Akimoto, H.: Kinetics of heterogeneous reactions of HO₂
931 radical at ambient concentration levels with (NH₄)₂SO₄ and NaCl aerosol particles., *J. Phys.*
932 *Chem. A*, 112, 2370-2377, <https://doi.org/10.1021/jp0769936>, 2008.

933 Taketani, F., Kanaya, Y., Pocharnart, P., Liu, Y., Li, J., Okuzawa, K., Kawamura, K., Wang,
934 Z., and Akimoto, H.: Measurement of overall uptake coefficients for HO₂ radicals by aerosol
935 particles sampled from ambient air at Mts. Tai and Mang (China). *Atmos. Chem. Phys.*, 12,
936 11907-11916, <https://doi.org/10.5194/acp-12-11907-2012>, 2012.

937 Tan, Z., Hofzumahaus, A., Lu, K., Brown, S. S., Holland, F., Huey, L. G., Kiendler-Scharr,
938 A., Li, X., Liu, X., Ma, N., Min, K.-E., Rohrer, F., Shao, M., Wahner, A., Wang, Y.,
939 Wiedensohler, A., Wu, Y., Wu, Z., Zeng, L., Zhang, Y., and Fuchs, H.: No Evidence for a
940 Significant Impact of Heterogeneous Chemistry on Radical Concentrations in the North
941 China Plain in Summer 2014, *Environ. Sci. Technol.*, 54, 5973-5979,
942 <https://doi.org/10.1021/acs.est.0c00525>, 2020.

943 Thornton, J. A. and Abbatt, J. P. D.: Measurements of HO₂ uptake of aqueous aerosol: Mass
944 accommodation coefficients and net reactive loss., *J. Geophys. Res.*, 110,
945 <https://doi.org/10.1029/2004JD005402>, 2005.

946 Thornton, J. A., Jaegle, L., and McNeill, V. F.: Assessing known pathways for HO₂ loss in
947 aqueous atmospheric aerosols: Regional and global impacts on tropospheric oxidants. , *J.*
948 *Geophys. Res.*, 113, <https://doi.org/10.1029/2007JD009236>, 2008.

949 van der A, R. J., Mijling, B., Ding, J., Koukouli, M. E., Liu, F., Li, Q., Mao, H., and Theys,
950 N.: Cleaning up the air: effectiveness of air quality policy for SO₂ and NO_x emissions in
951 China, *Atmos. Chem. Phys.*, 17, 1775-1789, <https://doi.org/10.5194/acp-17-1775-2017>, 2017.

952 Verstraeten, W. W., Neu, J. L., Williams, J. E., Bowman, K. W., Worden, J. R., and
953 Boersma, K. F.: Rapid increases in tropospheric ozone production and export from China,
954 *Nat. Geosci.*, 8, 690-695, <https://doi.org/10.1038/ngeo2493>, 2015.

955 Wang, P.: China's air pollution policies: Progress and challenges, *Current Opinion in*
956 *Environmental Science & Health*, 19, 100227, <https://doi.org/10.1016/j.coesh.2020.100227>,
957 2021.

958 Whalley, L. K., Blitz, M. A., Desservattez, M., Seakins, P. W., and Heard, D. E.: Reporting
959 the sensitivity of laser-induced fluorescence instruments used for HO₂ detection to an
960 interference from RO₂ radicals and introducing a novel approach that enables HO₂ and

961 certain RO₂ types to be selectively measured, *Atmos. Meas. Tech.*, 6, 3425-3440,
962 <https://doi.org/10.5194/amt-6-3425-2013>, 2013.

963 Whalley, L. K., Stone, D., Bandy, B., Dunmore, R., Hamilton, J. F., Hopkins, J., Lee, J. D.,
964 Lewis, A. C., and Heard, D. E.: Atmospheric OH reactivity in central London: observations,
965 model predictions and estimates of in situ ozone production, *Atmos. Chem. Phys.*, 16, 2109-
966 2122, <https://doi.org/10.5194/acp-16-2109-2016>, 2016.

967 Whalley, L. K., Stone, D., Dunmore, R., Hamilton, J., Hopkins, J. R., Lee, J. D., Lewis, A.
968 C., Williams, P., Kleffmann, J., Laufs, S., Woodward-Massey, R., and Heard, D. E.:
969 Understanding in situ ozone production in the summertime through radical observations and
970 modelling studies during the Clean air for London project (ClearLo), *Atmos. Chem. Phys.*,
971 18, 2547-2571, <https://doi.org/10.5194/acp-18-2547-2018>, 2018.

972 Whalley, L. K., Furneaux, K. L., Goddard, A., Lee, J. D., Mahajan, A., Oetjen, H., Read, K.
973 A., Kaaden, N., Carpenter, L. J., Lewis, A. C., Plane, J. M. C., Saltzman, E. S.,
974 Wiedensohler, A., and Heard, D. E.: The chemistry of OH and HO₂ radicals in the boundary
975 layer over the tropical Atlantic Ocean, *Atmos. Chem. Phys.*, 10, 1555-1576,
976 <https://doi.org/10.5194/acp-10-1555-2010>, 2010.

977 Whalley, L. K., Slater, E. J., Woodward-Massey, R., Ye, C., Lee, J. D., Squires, F., Hopkins,
978 J. R., Dunmore, R. E., Shaw, M., Hamilton, J. F., Lewis, A. C., Mehra, A., Worrall, S. D.,
979 Bacak, A., Bannan, T. J., Coe, H., Ouyang, B., Jones, R. L., Crilley, L. R., Kramer, L. J.,
980 Bloss, W. J., Vu, T., Kotthaus, S., Grimmond, S., Sun, Y., Xu, W., Yue, S., Ren, L., Acton,
981 W. J. F., Hewitt, C. N., Wang, X., Fu, P., and Heard, D. E.: Evaluating the sensitivity of
982 radical chemistry and ozone formation to ambient VOCs and NO_x in Beijing, *Atmos. Chem.*
983 *Phys. Discuss.*, 21, 2125-2147, <https://doi.org/10.5194/acp-2020-785>, 2021.

984 Wiedensohler, A., Birmili, W., Nowak, A., Sonntag, A., Weinhold, K., Merkel, M., Wehner,
985 B., Tuch, T., Pfeifer, S., Fiebig, M., Fjåraa, A. M., Asmi, E., Sellegri, K., Depuy, R., Venzac,
986 H., Villani, P., Laj, P., Aalto, P., Ogren, J. A., Swietlicki, E., Williams, P., Roldin, P.,
987 Quincey, P., Hüglin, C., Fierz-Schmidhauser, R., Gysel, M., Weingartner, E., Riccobono, F.,
988 Santos, S., Gröning, C., Faloon, K., Beddows, D., Harrison, R., Monahan, C., Jennings, S. G.,
989 O'Dowd, C. D., Marinoni, A., Horn, H. G., Keck, L., Jiang, J., Scheckman, J., McMurry, P.
990 H., Deng, Z., Zhao, C. S., Moerman, M., Henzing, B., de Leeuw, G., Löschau, G., and
991 Bastian, S.: Mobility particle size spectrometers: harmonization of technical standards and
992 data structure to facilitate high quality long-term observations of atmospheric particle number
993 size distributions, *Atmos. Meas. Tech.*, 5, 657-685, <https://doi.org/10.5194/amt-5-657-2012>,
994 2012.

995 Woodward-Massey, R., Slater, E. J., Alen, J., Ingham, T., Cryer, D. R., Stimpson, L. M., Ye,
996 C., Seakins, P. W., Whalley, L. K., and Heard, D. E.: Implementation of a chemical
997 background method for atmospheric OH measurements by laser-induced fluorescence:
998 characterisation and observations from the UK and China, *Atmos. Meas. Tech.*, 13, 3119-
999 3146, <https://doi.org/10.5194/amt-13-3119-2020>, 2020.

1000 Xue, L. K., Wang, T., Gao, J., Ding, A. J., Zhou, X. H., Blake, D. R., Wang, X. F., Saunders,
1001 S. M., Fan, S. J., Zuo, H. C., Zhang, Q. Z., and Wang, W. X.: Ground-level ozone in four
1002 Chinese cities: precursors, regional transport and heterogeneous processes, *Atmos. Chem.*
1003 *Phys.*, 14, 13175-13188, <https://doi.org/10.5194/acp-14-13175-2014>, 2014.

1004 Ye, C., Heard, D. E., and Whalley, L. K.: Evaluation of novel routes for NO_x formation in
1005 remote regions. , *Environ. Sci. Technol.*, 51, 7442-7449, <https://doi.org/acs.est.6b06441>,
1006 2017.

1007 Zhou, J., Murano, K., Kohno, N., Sakamoto, Y., and Kajii, Y.: Real-time quantification of the
1008 total HO₂ reactivity of ambient air and HO₂ uptake kinetics onto ambient aerosols in Kyoto
1009 (Japan), *Atmos. Environ.*, 223, 117189, <https://doi.org/10.1016/j.atmosenv.2019.117189>,
1010 2020.

1011 Zhou, J., Sato, K., Bai, Y., Fukusaki, Y., Kousa, Y., Ramasamy, S., Takami, A., Yoshino, A.,
1012 Nakayama, T., Sadanaga, Y., Nakashima, Y., Li, J., Murano, K., Kohno, N., Sakamoto, Y.,
1013 and Kajii, Y.: Kinetics and impacting factors of HO₂ uptake onto submicron atmospheric
1014 aerosols during the 2019 Air QUALity Study (AQUAS) in Yokohama, Japan, *Atmos. Chem.*
1015 *Phys.*, 21, 12243-12260, <https://doi.org/10.5194/acp-21-12243-2021>, 2021.

1016